

**OPEN ACCESS**

# Impact of Electrolyte Solvent on $\text{Li}_4\text{Ti}_5\text{O}_{12}/\text{LiNi}_{0.90}\text{Mn}_{0.05}\text{Co}_{0.05}\text{O}_2$ Battery Performance for Behind-the-Meter Storage Applications

To cite this article: Drew J. Pereira *et al* 2025 *J. Electrochem. Soc.* **172** 020527

View the [article online](#) for updates and enhancements.

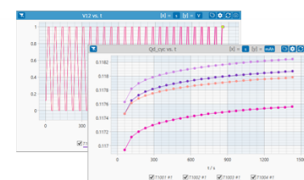
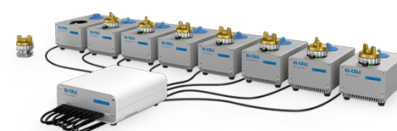
## You may also like

- [Mechanistic and Mitigation-Strategy Insights into NaCl and CaCl<sub>2</sub> Contamination of Proton-Exchange-Membrane Water Electrolysis Using Continuum Modeling](#)  
Arthur R. Dizon and Adam Z. Weber
- [Comprehensive Understanding of Accelerated Stress Test Protocols for Fe-N-C Catalysts in Acidic Aqueous Media](#)  
Hao-Ran Wu, Yuan Li, Miao-Ying Chen et al.
- [Fast-Charging Lithium-Ion Battery Protocols: LMFP Pouch Cells as a Rate Capability Case Study](#)  
Gerard Bree, Veronika Majherova, Eleni Fiamegkou et al.

## PAT-Tester-x-8 Potentiostat: Modular Solution for Electrochemical Testing!

**EL-CELL<sup>®</sup>**  
electrochemical test equipment

- ✓ **Flexible Setup with up to 8 Independent Test Channels!**  
Each with a fully equipped Potentiostat, Galvanostat and EIS!
- ✓ **Perfect Choice for Small-Scale and Special Purpose Testing!**  
Suited for all 3-electrode, optical, dilatometry or force test cells from EL-CELL.
- ✓ **Complete Solution with Extensive Software!**  
Plan, conduct and analyze experiments with EL-Software.
- ✓ **Small Footprint, Easy to Setup and Operate!**  
Usable inside a glove box. Full multi-user, multi-device control via LAN.



Contact us:

☎ +49 40 79012-734

✉ sales@el-cell.com

🌐 www.el-cell.com



# Impact of Electrolyte Solvent on $\text{Li}_4\text{Ti}_5\text{O}_{12}/\text{LiNi}_{0.90}\text{Mn}_{0.05}\text{Co}_{0.05}\text{O}_2$ Battery Performance for Behind-the-Meter Storage Applications

Drew J. Pereira,<sup>1,\*,z</sup> Maxwell C. Schulze,<sup>1,\*,z</sup> Yeyoung Ha,<sup>1</sup> Yicheng Zhang,<sup>1</sup> Jiyeon Gim,<sup>2</sup> Stephen E. Trask,<sup>2</sup> Ozgenur Kahvecioglu,<sup>3</sup> Glenn R. Teeter,<sup>1</sup> Anthony K. Burrell,<sup>1</sup> and Katharine L. Harrison<sup>1,z</sup>

<sup>1</sup>Materials, Chemical, and Computational Sciences Directorate, National Renewable Energy Laboratory, Golden, Colorado 80401, United States of America

<sup>2</sup>Chemical Sciences and Engineering Division, Argonne National Laboratory, Lemont, Illinois 60439, United States of America

<sup>3</sup>Applied Materials Division, Argonne National Laboratory, Lemont, Illinois 60439, United States of America

Behind-the-Meter Storage (BTMS) systems require dedicated development of battery materials that target long cycle life and low cost at the system level. Pairing  $\text{Li}_4\text{Ti}_5\text{O}_{12}$  (LTO) and  $\text{LiNi}_{0.9}\text{Mn}_{0.05}\text{Co}_{0.05}\text{O}_2$  (NMC90-5-5) shows promise to achieve targets for BTMS applications; however, minimal literature is available that discusses electrolyte solvent selection for this pairing. This study explores the role of electrolyte solvent on cycle life in LTO/NMC90-5-5 batteries. Four model electrolytes are evaluated; the baseline, Gen2, is compared with 1M  $\text{LiPF}_6$  added to each of three separate solvents: ethylene carbonate (EC), ethyl methyl carbonate (EMC), and fluoroethylene carbonate (FEC). An additional consideration is that NMC90-5-5 undergoes an H2→H3 phase transition that allows for a significant increase to capacity; however, it's unclear how this phase transition impacts electrolyte stability and cycle life. Therefore, the phase transition is avoided or accessed by cycling to 2.6V or 2.7V, respectively. The cells with Gen2, cycled to 2.6V, show the highest capacity retention due to EC passivating the LTO, EMC improving stability at the NMC90-5-5, and avoiding increased degradation from the 2.7V protocol. Despite having high initial reactivity that causes Li-depletion, FEC was the only solvent to avoid increased degradation when moving to the higher termination voltage.

© 2025 The Author(s). Published on behalf of The Electrochemical Society by IOP Publishing Limited. This is an open access article distributed under the terms of the Creative Commons Attribution 4.0 License (CC BY, <https://creativecommons.org/licenses/by/4.0/>), which permits unrestricted reuse of the work in any medium, provided the original work is properly cited. [DOI: 10.1149/1945-7111/adb51f]



Manuscript submitted December 21, 2024; revised manuscript received February 3, 2025. Published February 27, 2025.

Increasing generation of renewable energy and growing demand on the grid caused by electric vehicle (EV) charging warrants the development and implementation of behind-the-meter storage (BTMS) systems. BTMS is a stationary battery energy storage system on the consumer's side of the electric utility service meter that stores energy, including that of local intermittent sources like wind and solar, and supplements energy consumption during peak loads, reducing cost to the consumer and relieving strain on grid infrastructure.<sup>1</sup> Today, Li-ion battery development is primarily driven by the majority market share, EVs and portable electronics. However, BTMS batteries differ in their priorities, favoring low cost, safe operation, and long calendar/cycle life. While high volumetric energy density and high rate capability can be attractive for BTMS batteries, these metrics are not as critical due to the system's stationary nature, relatively lower space constraints, and large capacity. Additionally, BTMS batteries can be operated at elevated temperatures to improve kinetics as well as reduce thermal management cost. The BTMS batteries' unique priorities and operating conditions provide opportunity to explore alternative electrode and electrolyte materials.

Prior research evaluating battery chemistries for BTMS applications have focused on lithium titanate ( $\text{Li}_4\text{Ti}_5\text{O}_{12}$ , LTO) anodes paired with lithium manganese oxide ( $\text{LiMn}_2\text{O}_4$ , LMO) cathodes because they offer low cost, high safety, and long cycle life.<sup>2-4</sup> LTO and LMO contain earth-abundant materials, are critical-material-free, and have shown promise to be economically recyclable, leading to their relatively lower cost and confidence that supply will continue to be inexpensive moving forward.<sup>5-9</sup> LTO's safety characteristics come from its relatively lower heat release during thermal runaway, its suppressed formation of solid-electrolyte interphase (SEI), and its operating voltage (1.55V vs.  $\text{Li}/\text{Li}^+$ ) which mitigates growth of lithium dendrites.<sup>10-13</sup> LTO demonstrates impressive cycle life due to its spinel structure with negligible lithiation-driven volume

change (0.2%–0.3%), zero intrinsic strain, and again, suppressed formation of SEI.<sup>11-13</sup> LMO has performed well with relatively improved safety over other high-voltage chemistries<sup>14</sup> and recently demonstrated strong cycle life when paired with LTO in commercial cells, despite concerns of Mn dissolution.<sup>15</sup> However, LMO has a low volumetric energy density, and the additional space requirements translate to higher costs at the wholistic BTMS system scale. Additionally, as more modular BTMS systems are designed for space-constrained applications, there is a desire to explore the tradeoffs with alternative high-voltage cathodes that are more energy dense.

Layered metal oxide cathodes paired with LTO have promise to demonstrate high cycle stability and energy density; and to remain relevant for BTMS applications, cathodes with minimal or no “electric eighteen” critical materials,<sup>16</sup> like Co, have been explored. LTO has been paired with Li- and Mn-rich layered cathodes  $x\text{Li}_2\text{MnO}_3 \cdot (1-x)\text{LiMeO}_2$ , where Me = Ni, Mn, etc. (LMR-LM) and evaluated for BTMS applications.<sup>17,18</sup> Despite the findings that controlling upper voltage limit, prelithiating the electrode, and using ethylene carbonate (EC) -containing electrolytes all improve cycle life of LTO/LMR-LM batteries, the cycle stability was still inferior than that of LTO/LMO.<sup>17</sup>  $\text{LiNi}_{0.9}\text{Mn}_{0.1}\text{O}_2$  (NMC910) was also paired with LTO and evaluated as a critical material-free, high voltage system.<sup>19</sup> Though this system struggled to reach cycle stability needed for BTMS, fluoroethylene carbonate/ethyl methyl carbonate (FEC/EMC) co-solvent mixtures in the electrolyte outperformed conventional EC/EMC co-solvent mixtures in terms of cycling stability,<sup>19</sup> contrasting with findings in LTO/LMO<sup>4</sup> and LTO/LMR-LM<sup>17</sup> reports, which indicated that the decomposition products from EC were beneficial for passivating LTO. The discrepancy in the role of EC in these LTO systems with varying high-voltage cathodes highlights the complexity of how electrolyte design impacts cycle life for a given electrode pairing.

Motivated to maintain cycling stability while improving energy density of batteries for BTMS applications, another layered oxide is being explored as the LTO's cathode pairing,  $\text{LiNi}_{0.9}\text{Mn}_{0.05}\text{Co}_{0.05}\text{O}_2$  (NMC90-5-5). NMC90-5-5 is an economically-scaled, low-Co, and

\*Equal Contribution.

<sup>z</sup>E-mail: [drew.pereira@nrel.gov](mailto:drew.pereira@nrel.gov); [max.schulze@nrel.gov](mailto:max.schulze@nrel.gov); [katie.harrison@nrel.gov](mailto:katie.harrison@nrel.gov)

cost-effective material with high capacity from being able to access the H<sub>2</sub>→H<sub>3</sub> phase transition in Ni-rich layered oxides,<sup>20</sup> and with promise to improve capacity retention as inclusion of some Co reinforces layered ordering.<sup>21</sup> However, a primary concern for Ni-rich layered oxides for BTMS applications is the high voltage stability. Previously, Kim et al. applied an electrochemically-inert LMO coating to mitigate structural deterioration during cycling and prevent undesirable side reactions at the cathode/electrolyte interface, leading to improved capacity retention with the tradeoff of higher synthesis complexity and cost.<sup>22</sup> Unfortunately, BTMS's sensitivity to cost dictates the need for a different solution; and the engineering of electrolyte may be an option as a low-cost and elegant means to improve stability at the NMC90-5-5/electrolyte interface. Recently, Wang et al. used a figure-of-merit method to investigate electrolytes with varied additives, cosolvent ratios, and dual salts for graphite/NMC90-5-5 batteries; their comprehensive study underpins Gen2 (1.2M LiPF<sub>6</sub> in 3:7 EC:EMC) as a strong-performing electrolyte and presents the tradeoffs for electrolyte additives and dual salt systems.<sup>23</sup> However, LTO and graphite vary greatly in their impact on capacity retention due to key differences in their interaction with electrolyte. For example, LTO and graphite undergo different passivation processes.<sup>24,25</sup> Another example, graphite can uniquely be exfoliated, and the inclusion of EC in the electrolyte mitigates this issue,<sup>26</sup> while LTO doesn't have this constraint. Therefore, there is a need to investigate electrolytes for the BTMS-relevant LTO/NMC90-5-5 system.

The study presented here explores the role of electrolyte solvent on cycle life in LTO/NMC90-5-5 batteries for BTMS applications. Gen2, used as the baseline, is compared with 1M LiPF<sub>6</sub> added to each of three separate solvents: EC, EMC, and FEC. Each of these solvents provides advantages and disadvantages as potential single solvent electrolytes compared to Gen2. EC was chosen as a component in Gen2 that has been shown to be critical for passivating the LTO surface.<sup>2,4</sup> Additionally, high-viscosity EC-based electrolyte may be particularly promising in BTMS systems that operate at 45°C, keeping EC in its liquid state, and where safety is prioritized, by eliminating the highly flammable linear carbonate, EMC. EMC was chosen because it is also a component of Gen2 and because recent studies have suggested EMC-only electrolytes can improve performance of graphite/Ni-rich cathode cells when cycled to high potentials.<sup>27–29</sup> However, previous LTO/LMR-LM cell studies showed that EMC-only may not be compatible with LTO anodes.<sup>17,18</sup> The recent study of LTO/NMC910 cells with LiPF<sub>6</sub> in FEC/EMC mixed solvents suggest improvement in cycle life relative to Gen2, so FEC was selected as a single solvent electrolyte for the current study to compare to EC and EMC.<sup>19</sup> FEC is attractive because it exhibits good oxidative stability, is non-flammable, and has been shown to passivate interfaces with stable surface films.<sup>19,30,31</sup> Important to note is the H<sub>2</sub>→H<sub>3</sub> phase transition near the top of charge for NMC90-5-5, which results in severe structural distortions, as well as possible capacity loss.<sup>20,23</sup> The additional capacity from this phase transition is desirable, though it is not yet clear if the phase transition will decrease capacity retention below BTMS requirements. Because potential impacts degradation of the electrolyte solvents, the charge termination condition is also varied between 2.6V and 2.7V for LTO/NMC90-5-5 in this study. This termination voltage effectively prevents or allows access to the NMC90-5-5's H<sub>2</sub>→H<sub>3</sub> phase transition and affects electrolyte performance in both cases.

## Materials

**Synthesis of NMC90-5-5 active material.**—Ni<sub>0.90</sub>Mn<sub>0.05</sub>Co<sub>0.05</sub>(OH)<sub>2</sub> precursor powders were continuously synthesized using a 1L Taylor Vortex Reactor (Laminar) via hydroxide co-precipitation. This synthesis process was adapted from a previous report.<sup>32</sup> Desired amounts of NiSO<sub>4</sub>·6H<sub>2</sub>O (Sigma-Aldrich), MnSO<sub>4</sub>·H<sub>2</sub>O (Sigma-Aldrich), and CoSO<sub>4</sub>·7H<sub>2</sub>O (Sigma-Aldrich) salts were dissolved in nitrogen-purged, deionized (DI) water to target a 2M transition metal (TM) solution with

Ni:Mn:Co = 90:5:5 mole ratios. 4M NaOH (Sigma-Aldrich) and 4M NH<sub>4</sub>OH (Sigma-Aldrich) solutions were used as the co-precipitating and chelating agents in the co-precipitation synthesis, respectively. The pH of the solution inside the reactor was maintained at 11.92 (±0.02) throughout the reaction and the temperature was fixed at 52°C (±0.2°C). Prior to pumping in the reactants, the reactor was filled with nitrogen-purged DI water and the inner cylinder was rotated at 800 rpm to create a Taylor vortex flow pattern inside the gap between the two-concentric cylinders, where the reaction proceeds. The TM solution was fed at 1.67 ml/min and the NH<sub>4</sub>OH was fed at 0.83 ml/min during the synthesis process, while NaOH flow was set to maintain the pH of the solution. After steady state conditions were achieved, the product was collected with a continuous yield of ~17 g/hour until reaching the desired amount. The precipitated product was washed (with nitrogen-purged DI water until the conductivity of solution was below 20 μS/cm), filtered, and dried at 120°C in a vacuum oven overnight to obtain final hydroxides. The final hydroxide precursor had a tap density of 1.98 g/cm<sup>3</sup> with an average particle diameter of ~9 μm. The precursor mixture was prepared by thoroughly mixing the synthesized Ni<sub>0.90</sub>Mn<sub>0.05</sub>Co<sub>0.05</sub>(OH)<sub>2</sub> powder with finely ground LiOH·H<sub>2</sub>O (lithium hydroxide monohydrate, Sigma-Aldrich, 98% purity) in a Li-to-transition metal molar ratio of 1.01. The mixing process was carried out with a time-efficient acoustic mixer to avoid any unexpected oxidation of precursors. The prepared precursor mixture was transferred to pre-treated alumina crucibles, and they were placed in a stable (12-inch long) hot-zone within a multiple zone controlled tube furnace. The tube furnace was purged with oxygen gas for 2 hours before the calcination process at 720°C for 12 hours, while holding constant oxygen flow. The final NMC90-5-5 was then obtained after gently grinding the powder after a natural cooling. ICP-MS (Agilent 7850X) was employed to confirm TM molar ratios: Ni = 0.896, Mn = 0.051, and Co = 0.053.

**Electrodes.**—The electrodes evaluated in this work were provided by the Cell Analysis, Modeling, and Prototyping (CAMP) Facility at Argonne National Laboratory (ANL). The anode was comprised of 92 wt% LTO (Targray), 3 wt% conductive carbon (Timcal C-45), and 5 wt% polyvinylidene fluoride binder (PVDF, Kureha 9300). The LTO slurry was coated on a single side of 20 μm Al current collector yielding a coating thickness of 88 μm, coating loading of 13.13 mg/cm<sup>2</sup>, and porosity of 40.4%. Measured areal capacity for the LTO electrode was 2.00 mAh/cm<sup>2</sup> at a C/10 rate, where “C” represents the current needed to fully discharge the electrode in 1 hour, between 1.0–2.0V vs. Li/Li<sup>+</sup>. The cathode was comprised of 90 wt% NMC90-5-5 from the Synthesis of NMC90-5-5 Active Material section, 5 wt% conductive carbon (Timcal C-45), and 5 wt% PVDF binder (Solvay 5130). The NMC90-5-5 slurry was coated on a single side of 20 μm Al current collector yielding a coating thickness of 33 μm, coating loading of 9.16 mg/cm<sup>2</sup>, and porosity of 32.4%. Measured areal capacity for the NMC90-5-5 electrode was 1.83 mAh/cm<sup>2</sup> at a C/10 rate, between 3.0–4.3V vs. Li/Li<sup>+</sup>. The pairing of these electrodes results in an estimated N:P ratio of 1.09.

**Electrolytes.**—The electrolytes evaluated in this study include 1.2M LiPF<sub>6</sub> in 3:7 by wt% EC/EMC (Gen2), 1M LiPF<sub>6</sub> in ethyl methyl carbonate (EMC), 1M LiPF<sub>6</sub> in ethylene carbonate (EC), and 1M LiPF<sub>6</sub> in fluoroethylene carbonate (FEC). The electrolytes were chosen to be comparable with previous work on similar systems;<sup>2,18,19</sup> the highly-optimized Gen2 electrolyte serves as the high-performance baseline, while single-solvent electrolyte salt concentration was set to 1M for reasonable comparison and to avoid prohibitively high viscosity in cyclic carbonate solutions. It is worth noting here that each electrolyte solvent may be further optimized with a unique salt concentration, which is out of the scope of this study.

All electrolytes were prepared in an inert Ar glove box environment (Vacuum Atmospheres Company, <0.5 ppm O<sub>2</sub> and <0.5 ppm H<sub>2</sub>O). Gen2 and EC-based electrolytes were supplied as pre-mixed electrolytes (Tomiyama). EMC (Tomiyama) and FEC

(Tomiyama) were mixed with LiPF<sub>6</sub> salt (>99.99%, Sigma Aldrich) and stirred for at least 24 hours to make EMC and FEC-based electrolytes. All electrolytes were confirmed to be sufficiently dry (<20 ppm H<sub>2</sub>O) prior to cell assembly using Karl Fischer measurement (Mettler Toledo, C20S). A conductivity meter (Mettler Toledo FiveEasy F30) inside the glove box was used to measure conductivity of Gen2 (8.9 mS/cm), EMC-based (4.5 mS/cm), EC-based (2.3 mS/cm), and FEC-based (3.2 mS/cm) electrolytes at a reference temperature of 25°C.

## Methods

**Coin cell fabrication.**—The electrochemical testing in this study was performed on 2032-type coin cell assemblies (Hohsen Corp.) paired with the electrodes described in the Electrodes section. The anodes and cathodes were cut to 15 mm and 14 mm diameter discs, respectively. The LTO anodes and NMC90-5-5 cathodes were spot-welded (Sunstone CD160DPM2, 40 ws) directly to 15 mm diameter steel spacers with thicknesses of 0.5 mm and 1.0 mm, respectively. This spot-welding step encourages consistent assembly as well as consistent electrical contact with cell terminals throughout long-term cycling.

Full cells were assembled in an inert Ar glove box environment (Vacuum Atmospheres Company, < 0.5 ppm O<sub>2</sub> and < 0.5 ppm H<sub>2</sub>O), using the spacers spot-welded to electrodes and a wave spring (Hohsen Corp.) to apply pressure. During assembly, 30 μL of electrolyte was added on each side of the separator to help encourage separator and electrode wetting, totaling 60 μL of electrolyte. The separator used in this study was a 19 mm diameter trilayer (PP/PE/PP) separator (Celgard 2325) or nonwoven cellulose-based separator (delfort, Dreamweaver Gold 20), which has a fibrous structure that aids in wetting cell components—a requirement when using the high-viscosity EC and FEC-based electrolytes in this study. The cellulose-based separator was dried in a vacuum oven for 24 hours at 120°C to remove all moisture before assembly.<sup>33</sup>

**Electrochemical testing.**—All electrochemical testing was conducted in duplicate coin cells. Coin cells were tested at 45°C with a MACCOR Series 4000 Automated Test System in a MACCOR Model MTC-020 Temperature Chamber. Full cells were initially cycled on a BTMS-relevant formation and rate protocol that includes an initial 12 hour rest, then cycling (constant current—constant voltage, CCCV, charge with constant current, CC, discharge) at C/10, C/3, 1C, and 2C (3 cycles each). “C” represents the current needed to fully discharge the cell in 1 hour, and the “constant voltage” step involves holding the cell potential at the termination voltage until the current needed to maintain that voltage falls below a defined value, C/20 in this case. The value of “C” in the formation and rate test is based on the measured areal 1C capacity for the limiting NMC90-5-5 electrode, ~1.55 mA/cm<sup>2</sup>. The voltage range for the formation and rate test is either 1.4–2.6V (2.6V Protocol) or 1.4–2.7V (2.7V Protocol).

After the initial formation and rate protocol, the same cells were put on a BTMS cycling protocol which comprises the following sequence: 2 cycles at C/10 (CCCV charge until CV current falls below C/20, CC discharge), one hybrid pulse power characterization (HPPC) cycle, then 97 cycles at 1C (CCCV charge until CV current falls below C/20, CC discharge), where a new C-rate was defined by the practical 1C capacity of the same cell from the previous formation and rate test. C/10 and 1C cycles used voltage ranges of 1.4–2.6V (2.6V Protocol) or 1.4–2.7V (2.7V Protocol). The HPPC cycles were achieved by first charging at 1C, then discharging at 1C with current pulses applied in 10% depth of discharge increments. The current pulses included a 10 s discharge pulse at 2C, 40 s rest, a 10 s charge pulse at 1.5C, and 40 s rest. This 100 cycle sequence was repeated until reaching 1000 cycles.

**Post-mortem characterization.**—Some of the cells were disassembled after cycling and the unwashed electrodes were reassembled into half cells vs. Li metal (0.75 mm thickness, 15 mm diameter, 99.9%, Alfa Aesar) with 60 μL of pristine electrolyte of the same type used in the full cell during cycling. These were assembled in the same manner as the full cells from the Coin Cell Fabrication section, excepting that the Li metal would be pressed to a 0.5 mm spacer instead of 1 mm, to maintain a similar stack pressure as the full cells. Half cells were cycled between 1V and 2V for LTO and between 3V and 4.3V for NMC90-5-5. The half cells were cycled using the same C/10 rate from the full cell tests.

The rest of the cells were disassembled and their electrodes were extracted for characterization. The electrode samples were rinsed by soaking in 5 ml of dimethyl carbonate for 2 minutes, immediately followed by vacuum drying in the glove box antechamber for 1 hour. Scanning electron microscopy (SEM) was performed using a Hitachi S-4800 (acceleration voltage 6 kV, current 5 μA) on pristine and cycled LTO and NMC90-5-5 electrodes. X-ray photoelectron spectroscopy (XPS) was performed on a Physical Electronics 5600 instrument (monochromatic Al Kα X-ray excitation, hν 1.487 keV), and previously described<sup>34</sup> custom Igor Pro software was used for XPS data analysis.

## Results and Discussion

Several measurements and analyses are used in this study to evaluate the impact of electrolyte on battery performance, particularly cycling stability and interfacial electrode reactivity. To be concise, each measurement/analysis is described and discussed individually. Then, in the Confluence of Observations section, related observations are merged to provide further discussion and substantiate conclusions.

**Electrochemical performance.—Initial formation and rate.**—After assembly, the cells were first subjected to a combined formation and rate protocol. The resulting discharge capacities of each cycle are shown in the top row of Fig. 1. For the 2.6V protocol, the cells with Gen2 and EMC-based electrolytes display the highest capacity at all C-rates, with the EMC-based cells showing a negligibly lower capacity at the C/10 and 2C rates. The cells with EC-based electrolytes display marginally lower capacities than the Gen2 and EMC cells at lower rates, but the difference grows at higher rates, indicating a comparative performance limitation of the EC-based electrolyte that is supported by conductivity measurements and consistent with prior literature.<sup>2</sup> The cells with FEC-based electrolyte show a significantly lower capacity at all rates and larger drop in capacity when moving to higher rates, indicating that the FEC-based electrolyte is significantly performance limited, comparatively. In the case of all four electrolytes, a ~20% increase in C/10 capacity is observed when increasing the termination voltage from 2.6V to 2.7V, which is expected from the higher voltage allowing access to the H2→H3 phase transition plateau.<sup>20,23</sup> In the 2.7V termination protocol, the Gen2-based cells bracket the other better-performing electrolytes and the EC-based cells slightly outperform the EMC-based cells; however, the three cell types with non-FEC-based electrolytes exhibit similar performance. The cells with FEC-based electrolyte show lower performance than the other cells of a similar magnitude to that observed in the 2.6V protocol.

Coulombic efficiency (CE) of cycles can be used to compare parasitic reactivity in the cells. CE can be calculated using the following equation:

$$CE = \frac{\text{discharge capacity (Ah)}}{\text{charge capacity (Ah)}} \quad [1]$$

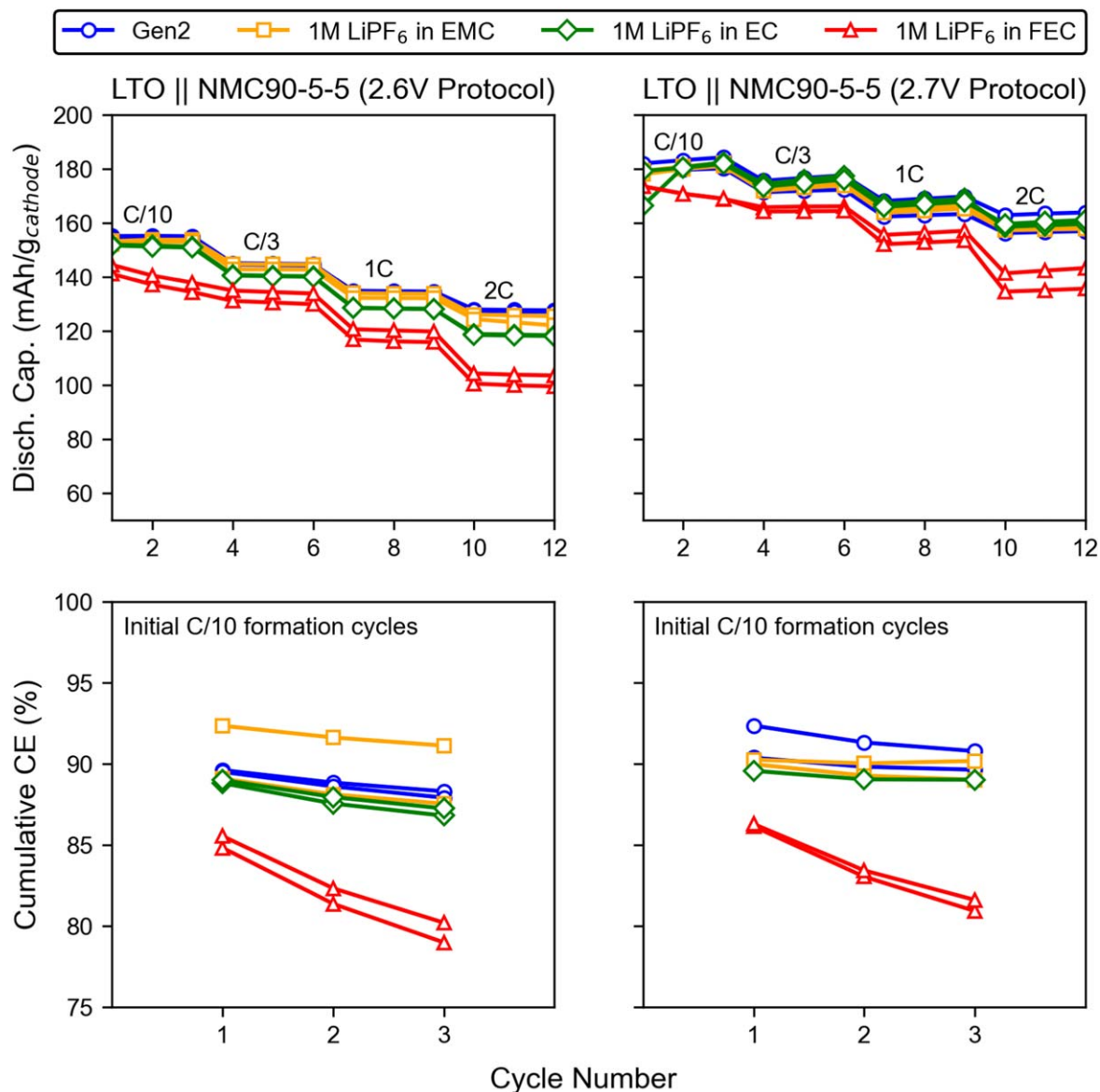


**Figure 1.** Comparison of duplicated cells during initial formation and rate protocol described in the Electrochemical Testing section. Discharge capacities are shown from each cycle (top) and calculations of cumulative coulombic efficiencies are shown from the first three C/10 cycles (bottom) of the formation and rate for cells under the 2.6V (left) and 2.7V (right) protocols.

where *CE* can be presented as a percentage by multiplying by 100%.

Cumulative coulombic efficiency can be calculated as the coulombic efficiency of the current cycle, *n*, multiplied by the coulombic efficiencies of all previous cycles:

$$\text{Cumulative CE} = \prod_{\text{cycle}=1}^n \text{CE}_{\text{cycle}} \quad [2]$$

where Cumulative CE can be presented as percentage by multiplying by 100%.

The bottom row of Fig. 1 shows the cumulative CE for each cells' first three C/10 cycles, which were chosen for comparison as these initial cycles play a significant role in the cell formation as well as the low rate being most useful for this comparison. It is worth noting that the CCCV charge/CC discharge protocol used here impacts the calculation of CE, and more evidence must be paired with this analysis before drawing conclusions. The main takeaway from the bottom row of Fig. 1 is that the cumulative CE for the FEC cells is significantly lower than all other cell types, which perform similarly. Additionally, the cumulative CE for the

FEC cells drop by a larger amount in the second and third cycles. This difference may indicate that the FEC is more reactive than the other electrolytes during formation, leading to reactions that cause electrode degradation, electrolyte dry-out, and/or depletion of Li inventory. It is worth addressing an outlier, one cell with EMC-based electrolyte under the 2.6V protocol, which displays a high cumulative coulombic efficiency compared to all other non-FEC-based cells. Closer inspection shows that this cell only displays slightly lower charge capacity in its first cycle, which may be attributed to minor differences caused by manual cell assembly. During subsequent cycling, its behavior converges with the other cells, giving confidence that it provides meaningful comparison for the rest of this study.

*Cycle life analysis.*—After the cells completed their formation and rate tests, they were placed on the cycle life protocol (Electrochemical Testing section). Primary data from the cycle life test are shown in Fig. 2, where the left side and right side show data from cells cycled under 2.6V and 2.7V protocols, respectively. The top row shows discharge capacities from every cycle, the middle row shows only the second C/10 “check-up” cycle in each 100 cycle

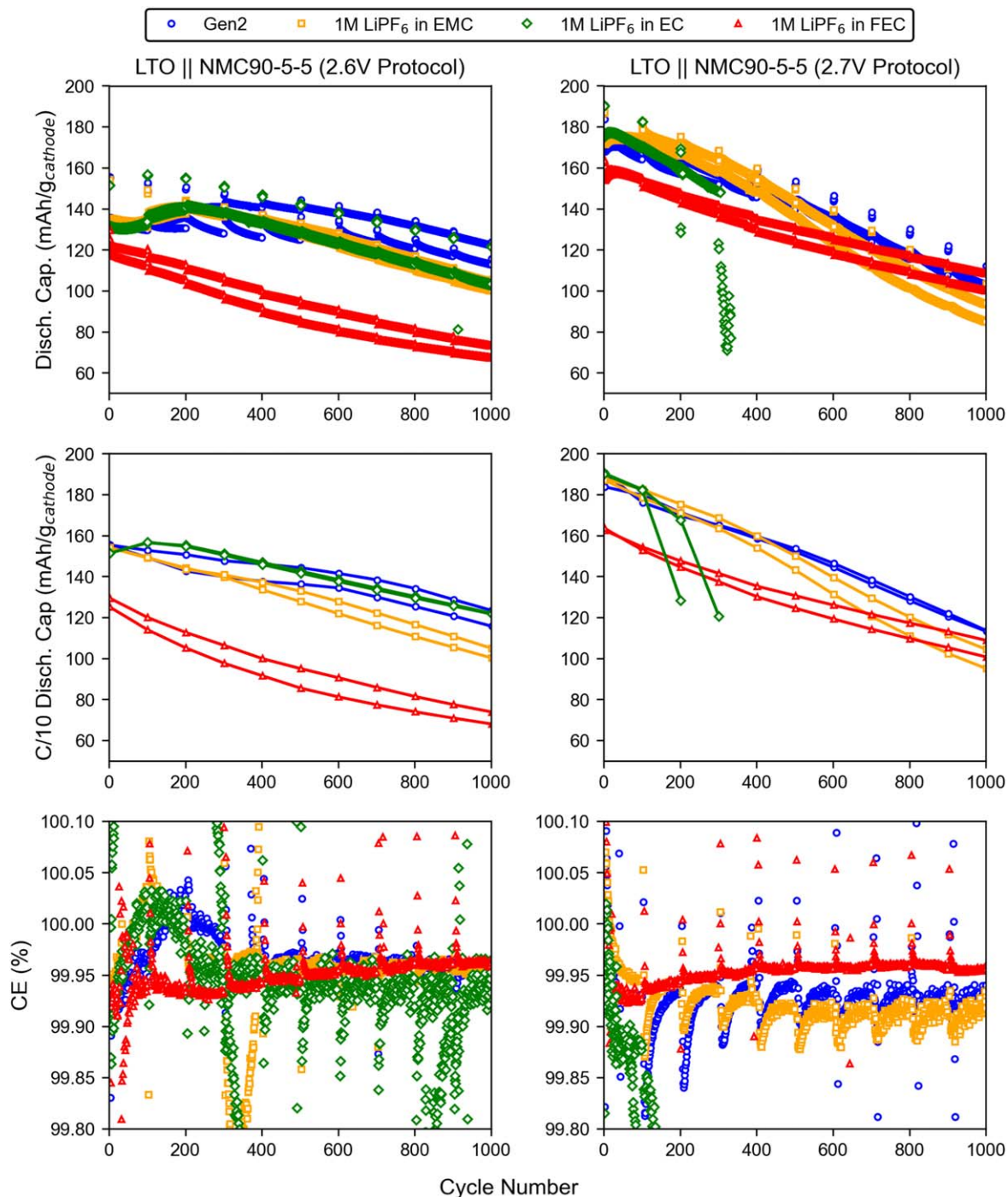


**Figure 2.** Cycle life comparison of duplicated cells assembled with four electrolytes cycled in the BTMS cycle life protocols with 2.6V (left) and 2.7V (right) termination voltages. See Methods Section for details regarding the cycle life protocol. Cycle 1 in these plots refers to the first cycle in the cycle life protocol, which follows the initial formation and rate test protocol that includes 12 prior cycles. The displayed data include discharge capacity of every cycle (top), discharge capacity of the second C/10 checkup cycle in each 100 cycle sequence (middle), and coulombic efficiency (CE) of each cycle (bottom).

sequence for clarity and to represent cell state-of-health, and the bottom row shows coulombic efficiency.

Generally, under the 2.6V protocol with 1C cycling, cells with Gen2 electrolyte display the the highest capacity retention; cells with EMC and EC-based electrolytes perform similarly, just below the Gen2 cells; and cells with FEC-based electrolytes show the lowest capacity retention in addition to a lower initial capacity compared to the other three electrolytes, likely due to the previously-discussed initial reactivity. Under the 2.6V protocol, the cells with Gen2 and EC-based electrolytes demonstrate the best state-of-health (C/10 capacity) at the end of cycling.

Under the 2.7V protocol, all cells show an increase in initial capacity of about 40 mAh/g, which again is expected from the higher voltage allowing access to the H<sub>2</sub>→H<sub>3</sub> phase transition plateau.<sup>20,23</sup> The cells with Gen2, EMC, and EC-based electrolyte show reduced capacity retention and state-of-health at the end of cycling, caused by an increase in the rate of capacity fade when moving from 2.6V to 2.7V protocols. The cells with EC-based electrolyte failed within the first 400 cycles, which may be caused by the poor oxidative stability of EC.<sup>35,36</sup> Interestingly, and despite the reduced initial capacity compared to the other cells, the cells with FEC-based electrolyte maintained a similar capacity retention as their 2.6V counterparts.

The result is that at the end of cycling, the cells with FEC-based electrolyte had similar 1C and C/10 discharge capacities compared to the cells with Gen2 and EMC-based electrolytes. Additionally, reasonable data extrapolation would suggest that the cells with FEC-based electrolyte would overtake the others with the highest 1C and C/10 capacities if cycled longer. This is also supported by the highest measured CE being achieved by the cells with FEC-based electrolyte, evidence that less parasitic reactions are occurring throughout cycle life. The cells with non-FEC-based electrolytes show lower CEs in the 2.7V protocol compared to 2.6V, which correlates to their higher capacity fade rates.

**Differential capacity ( $dQ/dV$ ) analysis.**—To better understand the mechanisms leading to capacity fade, differential capacity profiles are generated for the second C/10 “check-up” cycle in each 100 cycle sequence from the full cycle life tests. The resulting profiles for the cells cycled with 2.6V and 2.7V protocols are shown in Figs. 3 and 4, respectively. Locations for phase and phase changes

are inferred from previous literature on similar cathodes and labeled on the Gen2 plot.<sup>19,20</sup>

In consideration of cells cycled to 2.6V, the cells assembled with Gen2 exhibit relatively stable  $dQ/dV$  profiles, with a minor decrease of the low voltage peak at 2.15V. The cells with EMC and FEC-based electrolytes show similar trends in their  $dQ/dV$  signals, with low-voltage peaks diminishing and peak onsets shifting to higher potentials while higher-voltage peaks remain stable. Previous literature on another LTO system has attributed this shift to loss of lithium inventory caused by continuous electrolyte decomposition at the LTO during cycling, which is speculated to also be the case here.<sup>4</sup> Conversely, the cells with EC-based electrolyte exhibit notable decreases in the higher-voltage  $dQ/dV$  peaks, but no shifting of the lowest voltage peak at 2.05V. This supports prior evidence that EC helps to passivate the LTO anode,<sup>4</sup> while not having oxidative stability at higher potentials.<sup>35,36</sup>

More significant changes in the  $dQ/dV$  profiles are observed for the cells cycled using the 2.7V protocol (Fig. 4). The key difference

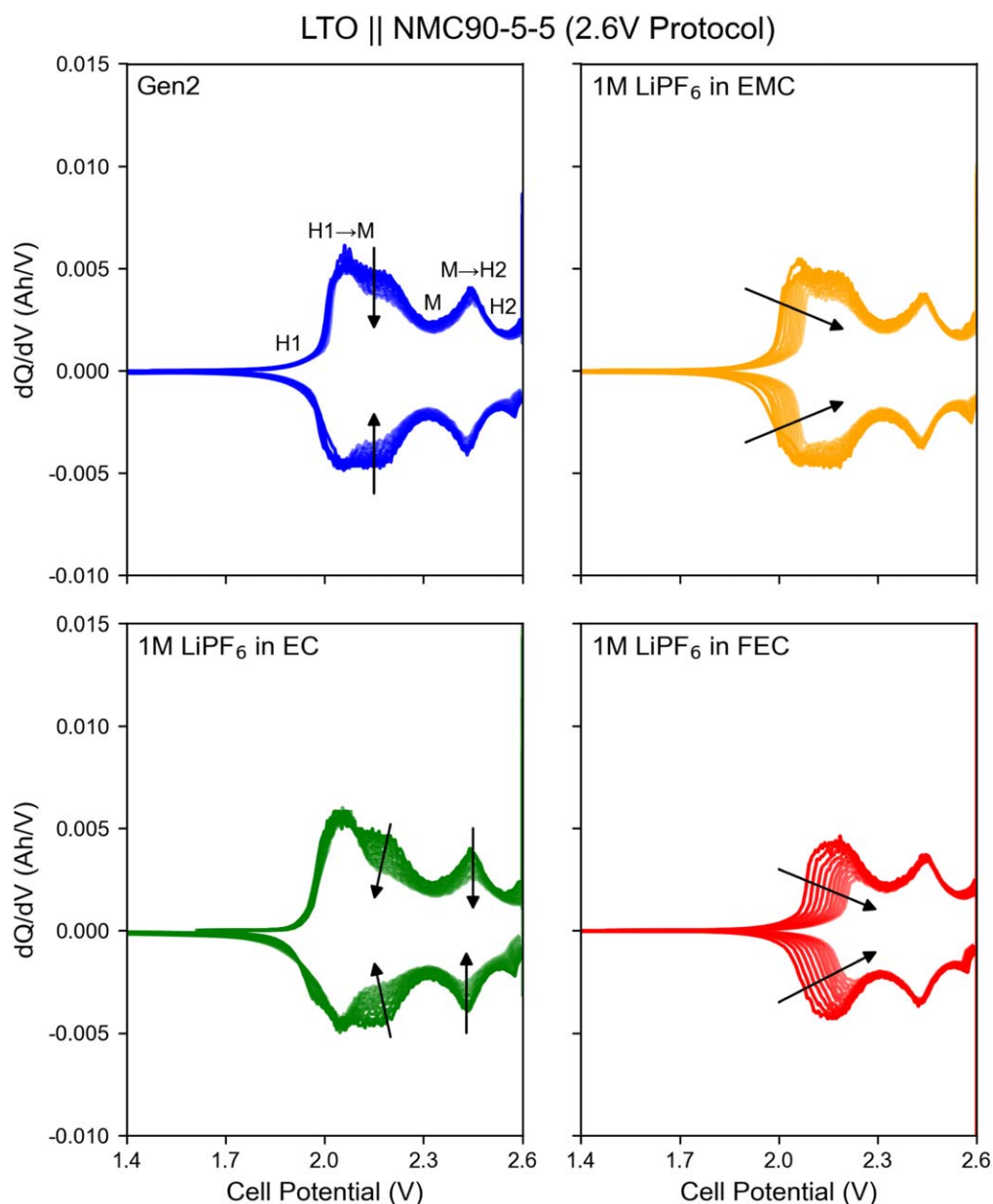


**Figure 3.** Differential capacity comparison for cells assembled with the four electrolytes, cycled in the BTMS cycle life protocol with 2.6V termination voltage. Each differential capacity profile represents the second C/10 checkup cycle in the 100 cycle sequence (cycles 2 to 1002, in 100 cycle increments). Arrows indicate cycling progression.

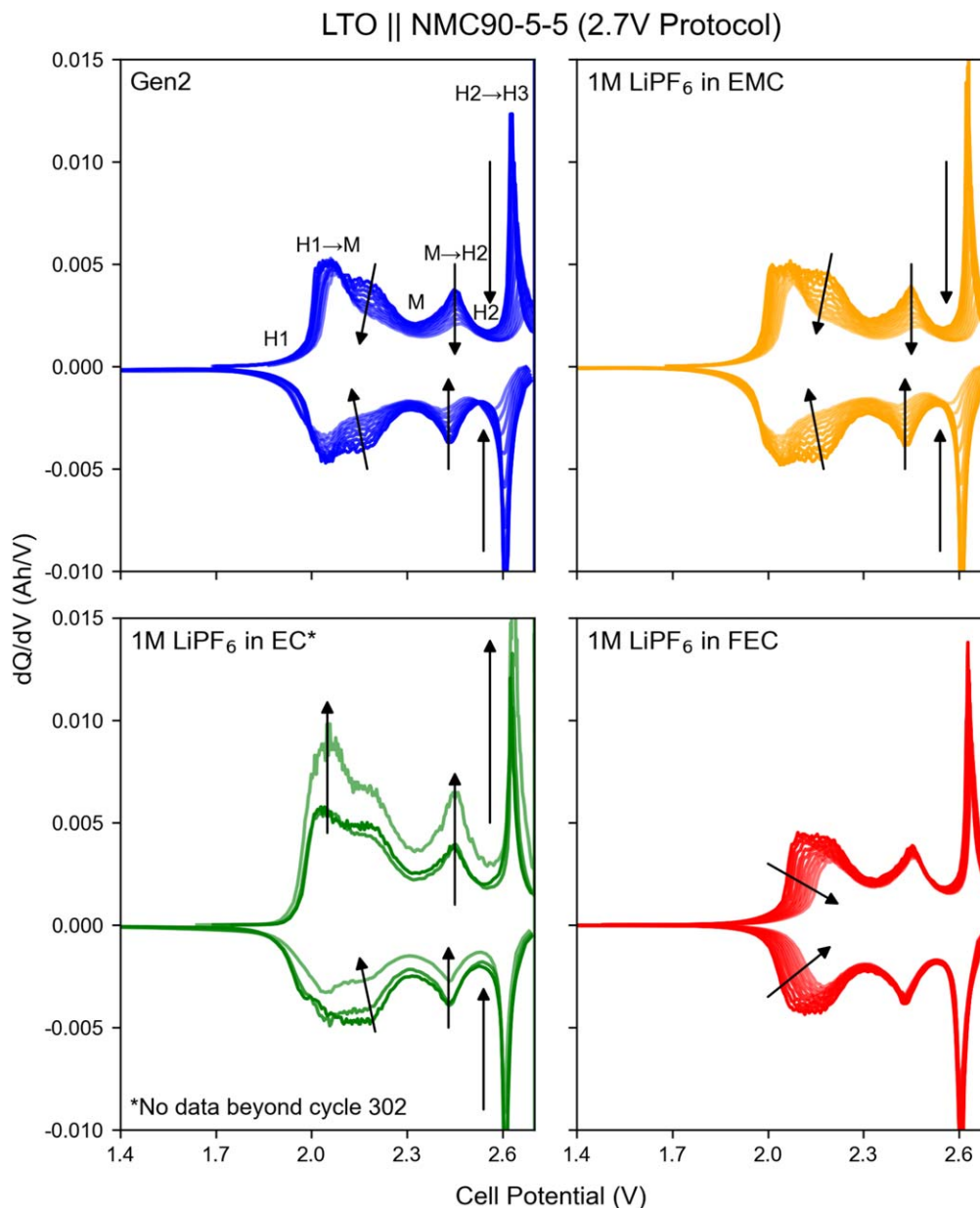


**Figure 4.** Differential capacity comparison for cells assembled with the four electrolytes, cycled in the BTMS cycle life protocol with 2.7V termination voltage. Each differential capacity profile represents the second C/10 checkup cycle in the 100 cycle sequence (cycles 2 to 1002, in 100 cycle increments). Arrows indicate cycling progression.

between 2.6V and 2.7V cells is the new peak that appears just after 2.6V. This peak represents a H2→H3 phase change in NMC90-5-5.<sup>23</sup> At the higher 2.7V protocol, all cells exhibit exacerbated degradation compared to 2.6V protocol, except cells with FEC-based electrolyte. The Gen2 cell exhibits similar behavior to the EC cells from the 2.6V protocol with a sharp decrease of the new H2→H3 peak, indicating degradation related to the newly-formed phase, or perhaps that the higher voltage is reaching the oxidative stability limit of EMC. The degradation related to H2→H3 transition includes mechanisms such as particle cracking, phase change, and reactivity with electrolyte.<sup>20,23</sup> The EMC cell also shows a degradation of its high-voltage peaks in addition to the low-voltage peak degradation already present in its 2.6V counterpart. The EC cell exhibits significant growth in charging signals, along with diminished discharging signals before failing altogether after checkup cycle 302. This demonstrates an extreme instability of EC under the 2.7V protocol, which is expected as the EC-based

electrolyte already demonstrated higher-voltage peak degradation in the 2.6V protocol. Most strikingly, the FEC cell exhibits the same diminishing low-voltage peak seen in the 2.6V protocol, but maintains the best electrochemical signals at high potentials. This indicates that the H2→H3 transition is more stable in FEC and that the access to the H3 phase does not degrade with cycling in FEC. This suggests that FEC is the least reactive with NMC90-5-5 at high potentials and/or that FEC decomposition products lead to the formation of a protective NMC90-5-5/electrolyte interphase, mitigating solid-electrolyte reactivity-related degradation.

*Areal specific impedance analysis.*—Calculated areal specific impedance (ASI) can be used to help visualize the initial impedance and impedance growth for each cell type. The ASI provides insight to the overall resistance growth in a cell, and can act as an indicator for the growth of passivating films on the electrode surfaces. The ASI is calculated by taking the change in voltage right before and at

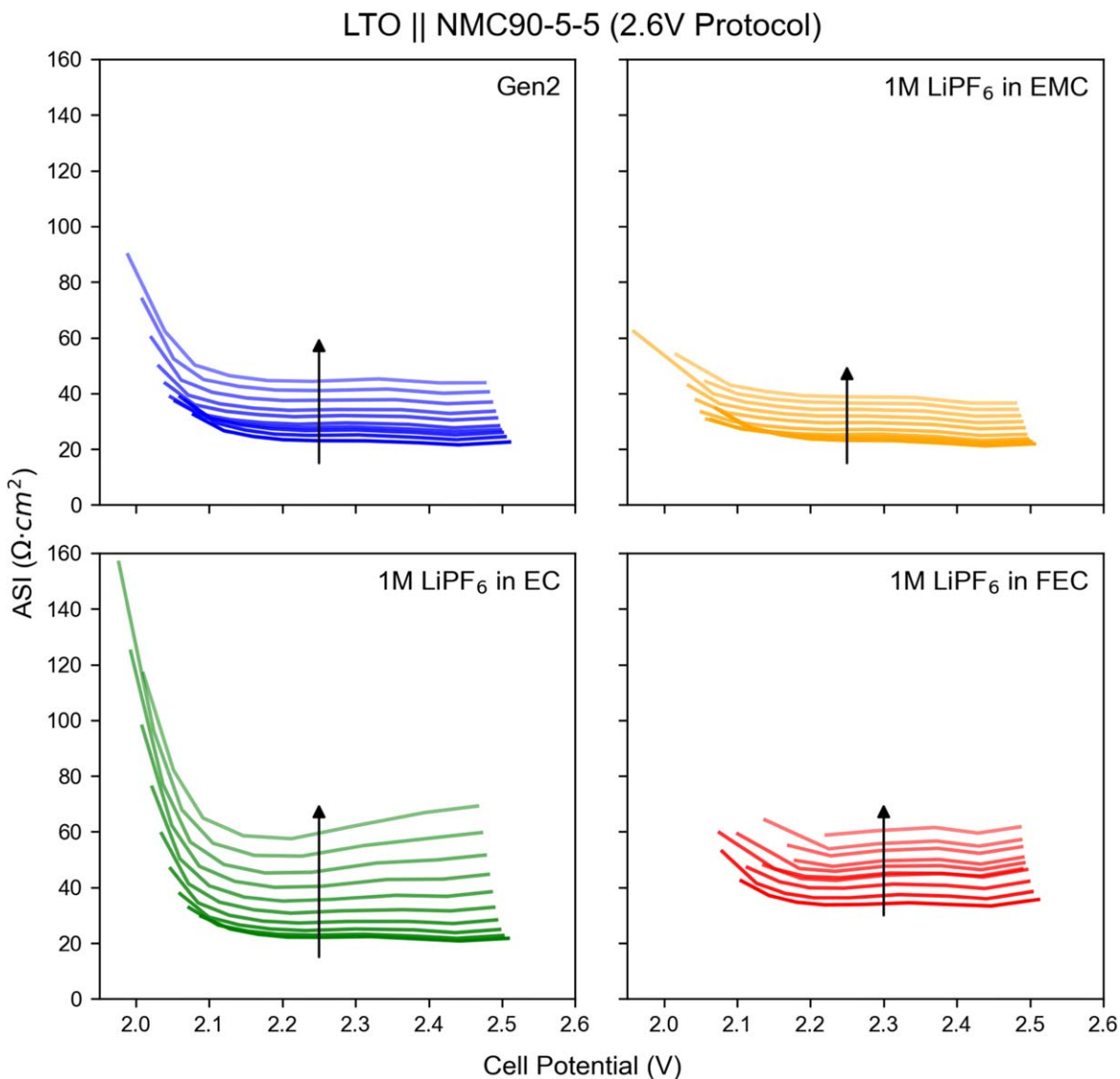


**Figure 5.** Areal specific impedance (ASI) against cell potential plotted for each HPPC cycle (cycles 3 to 903, in 100 cycle increments) for cells in the 2.6V BTMS cycle life protocol. Arrows indicate cycling progression.

the end of a pulse and dividing by the change in areal current density,  $I$ , at the same points:

$$ASI (\Omega \cdot \text{cm}^2) = \frac{\Delta V}{\Delta I} \quad [3]$$

The HPPC cycles, which are run every 100 cycles, contain several discharge pulses at incremental states of charge where ASI can be calculated. The resulting data for cells in 2.6V and 2.7V protocols is presented in Figs. 5 and 6, respectively.

For the 2.6V protocol, all the cells demonstrate a higher ASI at lower cell potentials, then level off at a lower, steady ASI as potential increases. Additionally, all cell ASI profiles gradually increase as the cells are cycled. The cell with the EMC-based electrolyte shows the lowest initial ASI, while cells with Gen2 and EC-based electrolyte show a similar initial ASI, just above that of the EMC. The cell with FEC-based electrolyte shows a significantly higher ASI, almost double the magnitude of the EMC-based electrolyte. As cells are cycled, the EMC cells show the lowest increase in ASI, Gen2 and FEC cells show a slightly larger increase, and EC cells increase the highest.

For the 2.7V protocol, Gen2, EMC and EC-based electrolytes all show a similar initial ASI, while FEC-based electrolyte shows the highest initial ASI, again. However, upon cycling, significantly different behavior is observed. First, EC cells failed after cycle 303, but showed the highest growth of ASI before failure. Gen2 and EMC-based electrolytes show significant growth to ASI upon cycling. Finally, FEC showed similar, but slightly increased, ASI growth to its 2.6V counterpart.

**Post-mortem characterization.—Half cell analysis.**—After completing their cycling protocols, cells were disassembled and the anode and cathode from some were each re-assembled into half cells (Post-mortem Characterization section) to evaluate health of the individual electrodes.

Figure 7 shows the voltage profile from the first C/10 cycle for each half cell. For the LTO electrodes, results are largely independent of the cycling protocol used, indicating that the increase of the upper termination voltage minimally affects the anode. LTO from cells assembled with EC-based electrolyte show the highest capacity, and thus, have the least amount of degradation, agreeing with

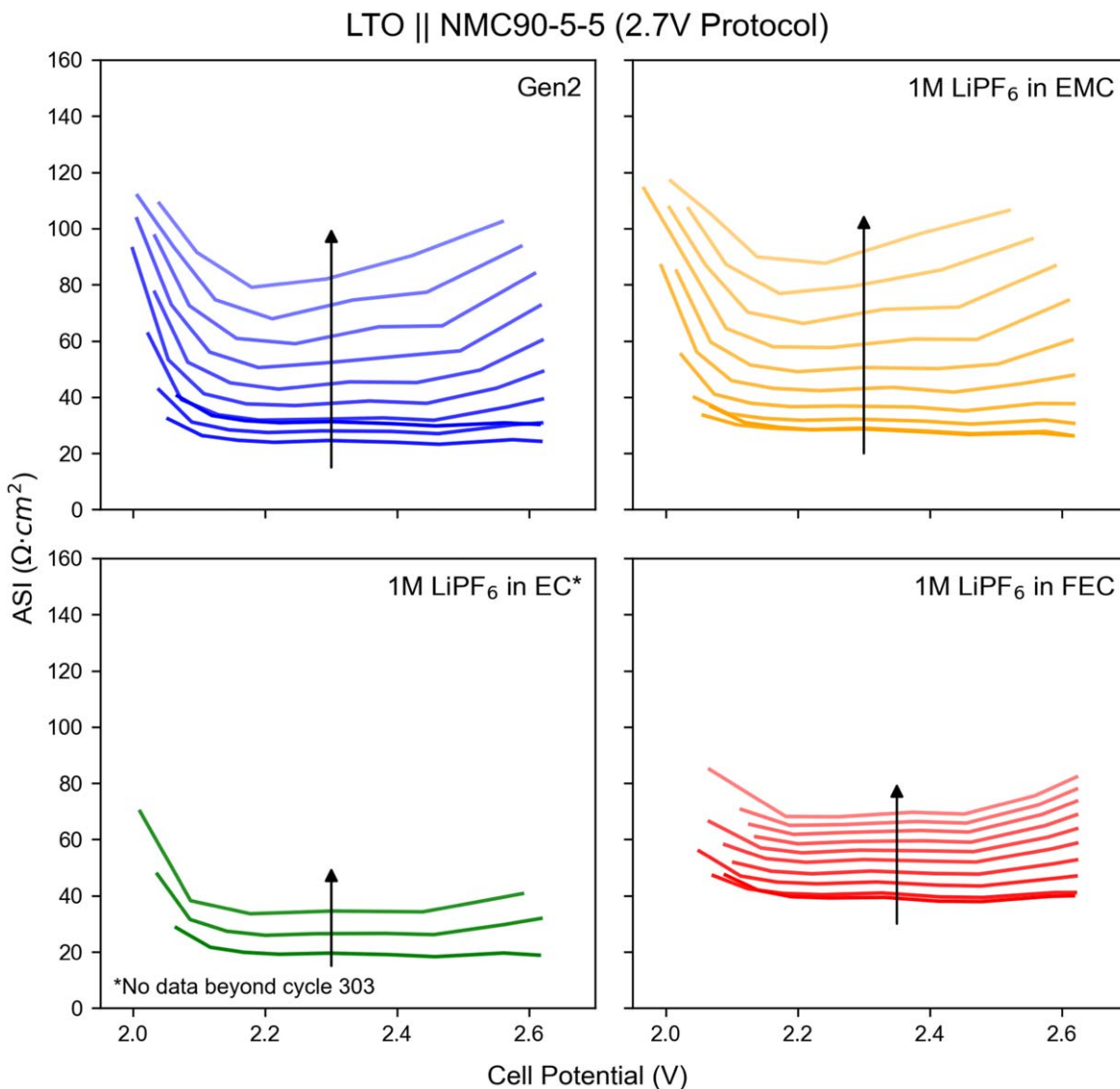


**Figure 6.** Areal specific impedance (ASI) against cell potential plotted for each HPPC cycle (cycles 3 to 903, in 100 cycle increments) for cells in the 2.7V BTMS cycle life protocol. Arrows indicate cycling progression.

results in literature that indicate EC passivates the LTO effectively.<sup>4</sup> The LTO electrodes from cells with Gen2 and EMC-based electrolytes show the next highest capacities. Despite having fresh electrolyte, the LTO from the cell cycled with FEC electrolyte has a notable drop in capacity compared to the EC-based electrolytes. This suggests that the electrode-electrolyte interactions from these cells cause direct degradation to the LTO active material, in addition to (or instead of) the degradation of the electrolyte itself. However, even at the end-of-life, the LTO was not the limiting electrode in terms of capacity in both protocols, so the significant degradation of the LTO would not be as noticeable in the full cell.

Shifting focus to the NMC90-5-5 half cells, there is a clear impact of the termination voltage on degradation. For the cells cycled on the 2.6V protocol, the NMC90-5-5 from cells with Gen2 and EMC-based electrolyte show the highest capacity, while the electrodes from EC and FEC cells show the lowest capacity. However, when moving to the 2.7V protocol, the Gen2 and EMC electrodes shift to now having the lowest capacity. This suggests that accessing H2→H3 phase change impacts how these electrolytes interact with (and degrade) the NMC90-5-5 active material. Interestingly, the NMC90-5-5 from the cells with FEC-based electrolyte shows consistent amounts of degradation between the

2.6V and 2.7V protocols, suggesting that the H2→H3 phase change does not degrade the NMC90-5-5 with the FEC, or that FEC's decomposition products form a passivation layer on the electrode surface that prevents further reactivity. Because the EC cells failed before 400 cycles in the 2.7V protocol, conclusions can't be formed from comparing the 2.6V and 2.7V protocol data.

*X-ray photoelectron spectroscopy.*—XPS can be used to further probe interfacial chemistry of the cycled electrodes. Figures 8 and 9 show the XPS spectra for pristine and post-mortem LTO and NMC90-5-5 electrodes, respectively. For peak assignments, a previously-described analysis method was used that relates an individual component's binding energy and intensity in several spectra to determine its contribution to spectra with overlapping peaks.<sup>34</sup> Only electrodes that underwent the 2.7V protocol were evaluated.

Spectra in Fig. 8 provide insight into the electrolyte reactivity and film formation at the LTO anode. In the XPS spectra taken from the pristine LTO anode, signals for PVDF, C45, LTO, and some contaminants are seen. The electrode cycled in EMC shows a strong Ti 2p and weak C-O species signals, indicative of a very thin and/or porous SEI. Gen2 and EC electrodes show minimal or no Ti 2p

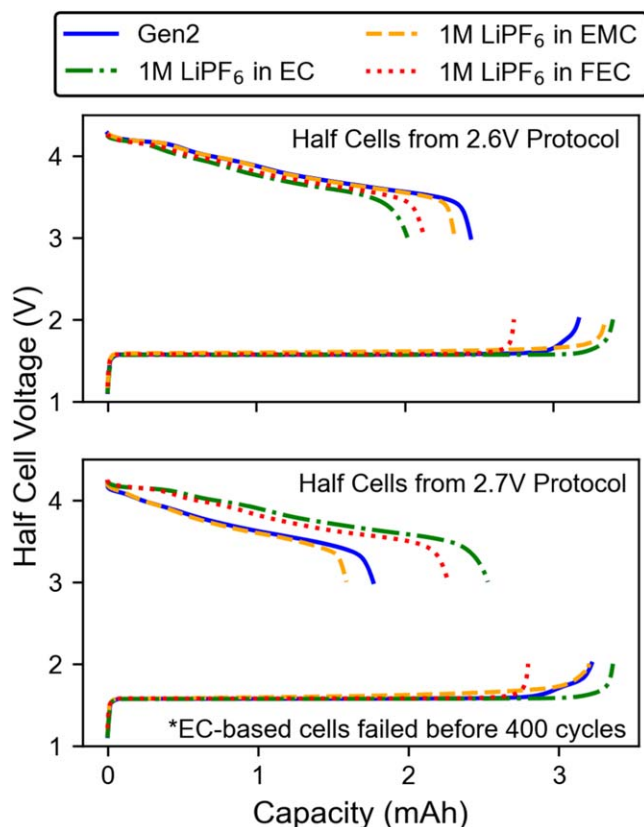


**Figure 7.** Comparison of voltage profiles from LTO and NMC90-5-5 half cells, whose electrodes were extracted from full cells that had been cycled under 2.6V (top) and 2.7V (bottom) BTMS cycle life protocols. Half cells were assembled with the same electrolytes from the full cell and cycled between 1–2 V for LTO and 3–4.3 V for NMC90-5-5. See Post-mortem Characterization section for more details about half cell assembly and testing.

signal, indicating that the presence of EC may lead to the formation of a relatively thick/dense film on the LTO surface. However, it should be noted that the possible presence of a small signal for  $\text{LiPF}_6$  in the EC electrode may indicate that the absence of Ti 2p signal could be due to residual electrolyte. The Gen2 and EMC electrodes show strong fluorophosphate peaks, which may mean that the presence of EMC leads to more  $\text{LiPF}_6$  degradation and/or that EC and FEC cells with nonwoven, cellulose-based separator have reduced hydrolysis due to their separator's  $\text{H}_2\text{O}/\text{HF}$  scavenging capability.<sup>33</sup>

Spectra in Fig. 9 provide insight into the electrolyte reactivity and film formation at the NMC90-5-5 cathode. In the XPS spectra taken from the pristine NMC90-5-5 cathode, signals for PVDF, C45, and some contaminants are present again. The FEC cathode uniquely shows strong C-O species, carbonate, and LiF signals, while showing no/minimal signals from PVDF or C45, indicating formation of thick/less porous SEI. An additional carbonate peak also shows up in the FEC spectra, which may have implications on surface passivation.

**Scanning electron microscopy.**—Scanning electron microscopy (Post-mortem Characterization section) was employed to visually observe the impact of electrolyte on the surface morphology of electrodes. Figure 10 shows representative images taken of the pristine LTO anode in addition to the post-cycled (2.7V protocol) anodes from cells with the four electrolytes evaluated in this study. Three magnifications are shown for each sample, capturing features of the electrode microstructure (top), a single secondary particle (middle), and several primary particles (bottom). The lower magnification images of the pristine anode show agglomerates of secondary particles ranging from 2–10  $\mu\text{m}$  in diameter. The anodes from Gen2, EMC, and FEC-based electrolytes all appear to be relatively similar in structure to the pristine sample. The clear outlier here is the cell with EC-based electrolyte, which appears to have a very thick, polymeric film that covers up details of the electrode microstructure, despite having experienced relatively fewer cycles.

Seen at the smallest scale is a collection of clearly defined primary particles of various sizes with sharp edges for the pristine

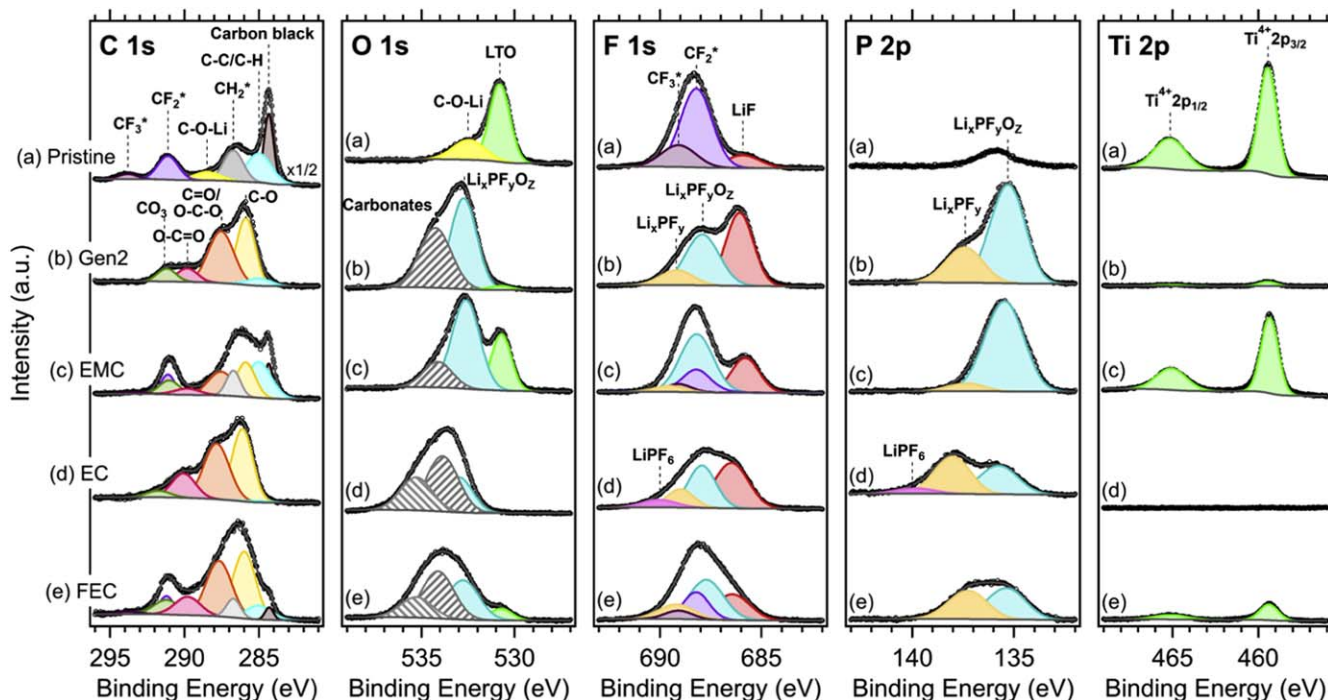


**Figure 8.** High-resolution C 1s, O 1s, F 1s, P 2p, and Ti 2p core-level XPS spectra of the (a) pristine LTO anode and LTO anodes from full cells cycled according to the BTMS cycle life protocol, terminated at 2.7V, with (b) Gen2, (c) 1M  $\text{LiPF}_6$  in EMC, (d) 1M  $\text{LiPF}_6$  in EC, and (e) 1M  $\text{LiPF}_6$  in FEC electrolytes. Note: cells with 1M  $\text{LiPF}_6$  in EC failed before reaching 400 cycles.

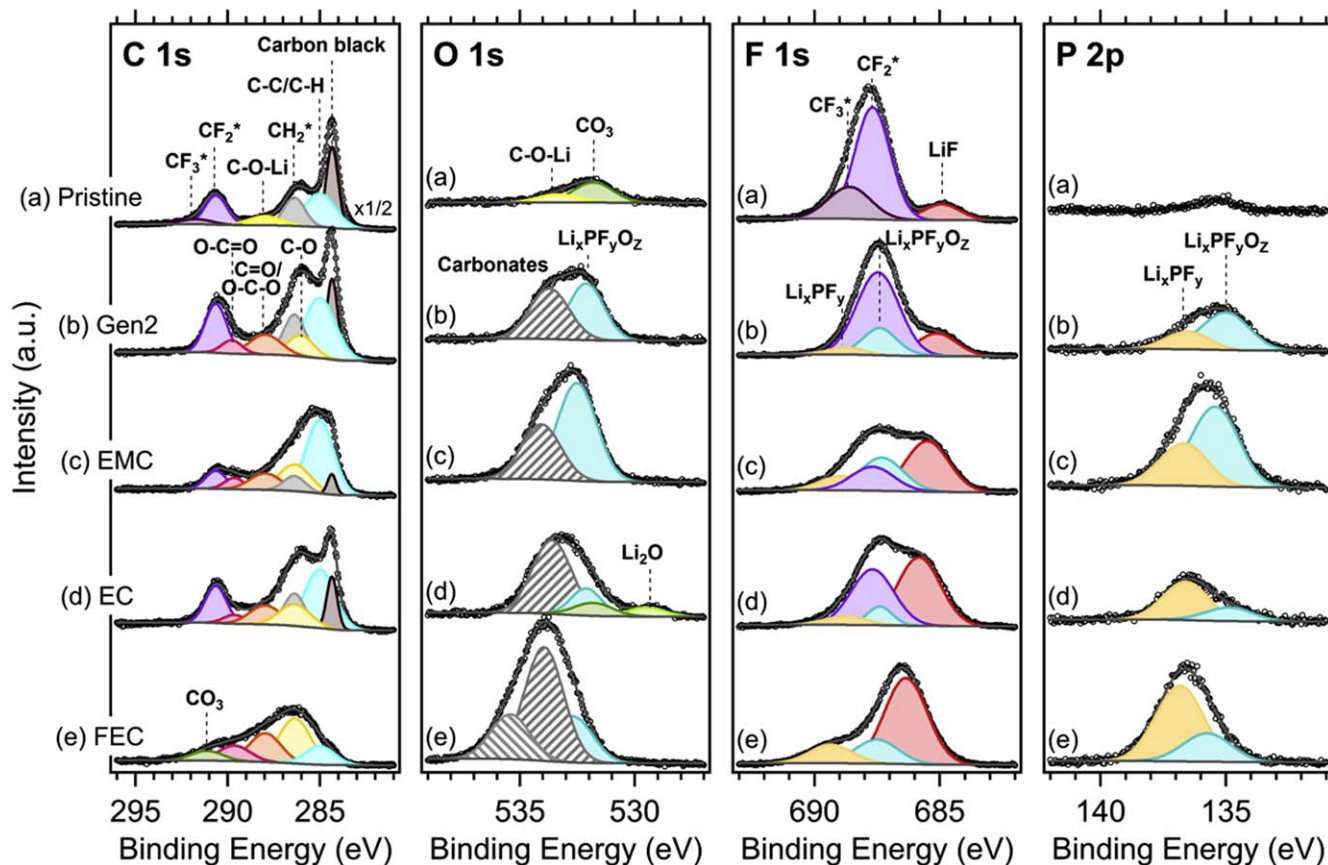


**Figure 9.** High-resolution C 1s, O 1s, F 1s, P 2p, and Ti 2p core-level XPS spectra of the (a) pristine NMC90-5-5 cathode and NMC90-5-5 cathodes from full cells cycled according to the BTMS cycle life protocol, terminated at 2.7V, with (b) Gen2, (c) 1M LiPF<sub>6</sub> in EMC, (d) 1M LiPF<sub>6</sub> in EC, and (e) 1M LiPF<sub>6</sub> in FEC electrolytes. Note: cells with 1M LiPF<sub>6</sub> in EC failed before reaching 400 cycles.

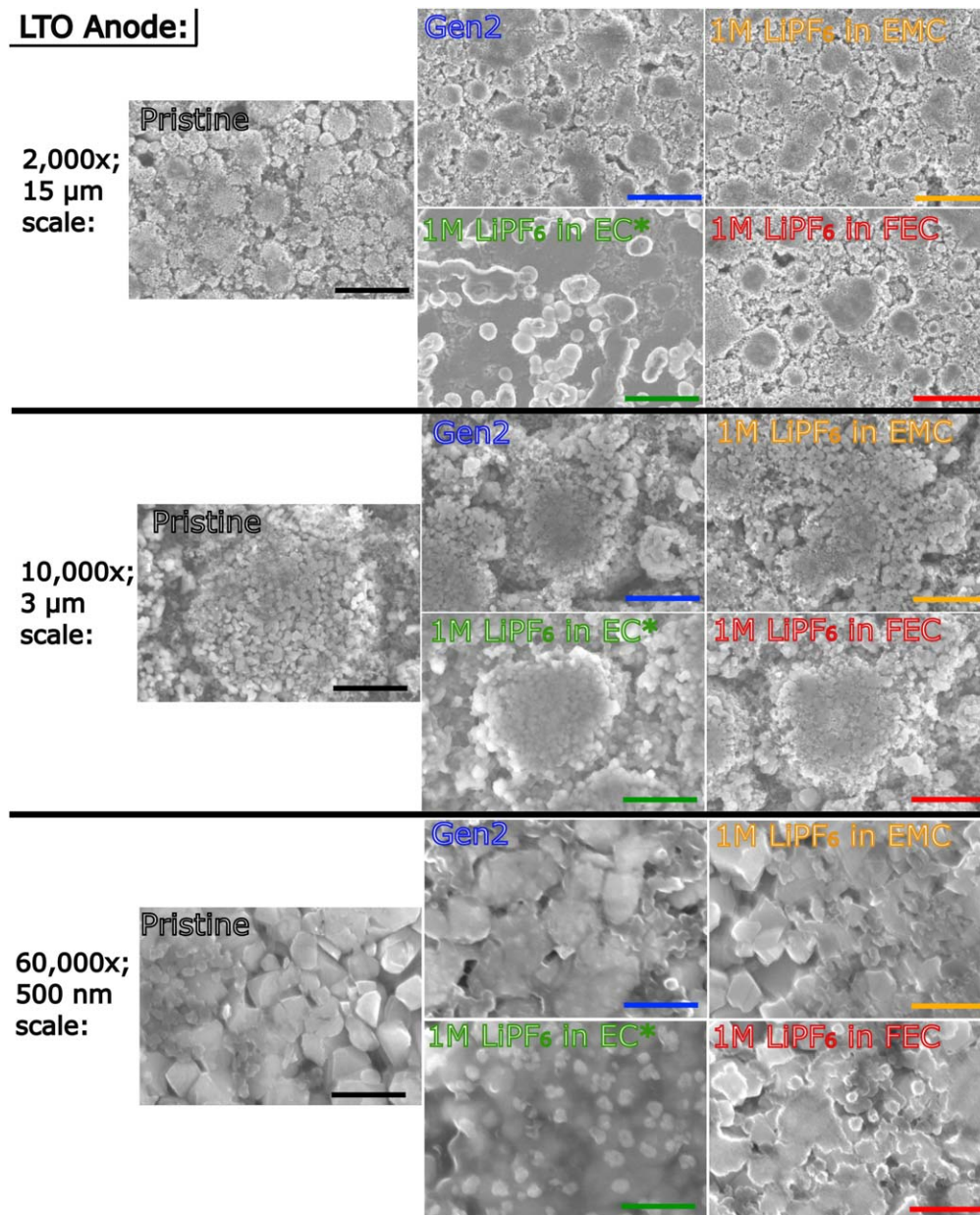
sample. At this scale, the anode from cells with 1M LiPF<sub>6</sub> in EMC looks the most similar to the pristine sample. The anodes from Gen2, EC, and FEC all have a significant loss of facets and features compared to the pristine sample, likely indicating a thicker SEI, but they qualitatively look different from each other. The Gen2 sample shows relatively continuous clear film on the surface of electrode, while still having some separation of the film between large primary particles. The EC sample has an almost completely continuous film on its surface, with gaps between primary particles filled in. Both of these may be indicative of a conformal SEI, possibly due to a primarily polymeric composition that successfully separates the electrolyte from the active material. However, it should be noted again here that in the 2.7V protocol, the EC failed early, so the EC electrode is not comparable in terms of total cycles, and the film morphology may continue to change over longer cycling. The FEC samples also have a thick film layer, however, the film doesn't seem to be continuous as there are crevices with high-contrast edges. The presence of a thick, porous film may indicate that the film itself is not stable and/or that the film morphology allows continued degradation due to electrolyte having direct access to the LTO surface throughout cycling.

Figure 11 shows analogous representative SEM images from the NMC90-5-5 cathodes at similar magnifications. At the lower magnifications, electrodes from Gen2, EC, and EMC-based cells all show a microstructure that largely resembles that of the pristine sample. The outlier is the electrode microstructure from the NMC90-5-5 with FEC-based electrolyte, where there is a noticeable accumulation of decomposition products collecting between secondary particles. Looking closer at the secondary particle reveals a film shrouding its edges and removing clarity of primary particle structure underneath. Looking in closer to the primary particles, for

the image from the pristine sample, several secondary particles are seen with a clear view of facets and features. The EC sample looks similar to its LTO counterpart, a loss of facets and features with gaps between secondary particles filled in. Again, EC cells prematurely failed, so morphology may change if cycled fully. The SEM from Gen2 and EMC samples show similar results; there is some loss of secondary particle clarity caused by what seems to be a somewhat nonuniform film on the particle surface, where the non-uniformity is observed as high-contrast, flaky features. The SEM of the FEC sample shows the most loss of facets and features, again suggesting significant film growth. The uniformity of the film and absence of conforming to the features suggest that the film is thick enough to fill in between most primary particle features.

**Confluence of observations.**—This final discussion section is written with the purpose to merge discussion from individual observations to produce more convincing conclusions with focus on how each electrolyte impacts battery longevity. In the four upcoming sections, each electrolyte is summarized and comparison is provided. Figure 12 is provided to illustrate this comparison.

**1M LiPF<sub>6</sub> in FEC.**—At a high level, the cells with 1M LiPF<sub>6</sub> in FEC seemingly show the lowest performance among all electrolytes. In particular, they display relatively lower low-rate and high-rate capacities from the rate test (Fig. 1), similar to the capacities in the initial portion of the cycle life tests (Fig. 2). This lower initial capacity is hypothesized to be caused by the high reactivity of the FEC in early cycles, leading to depletion of Li inventory. This hypothesis is supported by the significantly lower cumulative CE from the first three C/10 cycles (Fig. 1), which indicates relatively more parasitic reactivity that could be depleting Li inventory during



**Figure 10.** SEM images of the electrode microstructure (top), a single secondary particle (middle), and several primary particles (bottom) from the pristine LTO anode and LTO anodes from full cells cycled according to the BTMS cycle life protocol, terminated at 2.7V, with Gen2, 1M LiPF<sub>6</sub> in EMC, 1M LiPF<sub>6</sub> in EC, and 1M LiPF<sub>6</sub> in FEC electrolytes. \*Cells with 1M LiPF<sub>6</sub> in EC failed before reaching 400 cycles.

key formation cycles. It is also hypothesized that high-reactivity of FEC leads to the formation of a thick film on the electrode surfaces as illustrated in Fig. 12; which is supported by visual observation in the SEM images (Figs. 10 and 11); comparatively high initial ASI that can result from thick surface film (Figs. 5 and 6); and the minimal presence of carbon black in the electrodes' surface layers, per the XPS spectra (Figs. 8 and 9). However, despite the relatively high initial ASI, it is evident that the surface film formed in these cells is not too resistive for BTMS operating parameters, as the capacities from 1C cycling and C/10 checkup cycles show little to no difference.

While the comparatively low capacity in the cells with FEC-based electrolytes limits its use in BTMS applications, some behavior of the FEC provided a unique advantage over the other electrolytes. In particular, the FEC-based cells retained similar levels of capacity retention in both the 2.6V and 2.7V protocols, while all other cells showed decreased retention when moving to the higher termination

voltage. The hypothesis for why this occurs is that the high initial reactivity of the FEC leads to the deposition of its decomposition products on the surface of the NMC90-5-5. Compared to films on NMC90-5-5 from other electrolytes, the surface film from these FEC decomposition products is relatively more continuous, relatively thicker, and/or relatively more chemically stable. One or some combination of these attributes may help protect against further reactivity from high voltage at the NMC90-5-5. Therefore, the only degradation is occurring at the LTO, which wouldn't be impacted by changing the upper termination voltage. This hypothesis is supported by many results. First, FEC-based cells have similar, high coulombic efficiencies in the 2.6V and 2.7V protocols, indicating relatively and consistently low parasitic reactivity during cycling, excepting in initial formation cycles that likely form the stable surface film, as evident in Fig. 1. The FEC-based cells' dQ/dV profiles show a similar, consistent shifting/degradation of the low-voltage peak associated with the LTO, while maintaining the H2→H3 peak in the 2.7V profile, unlike other

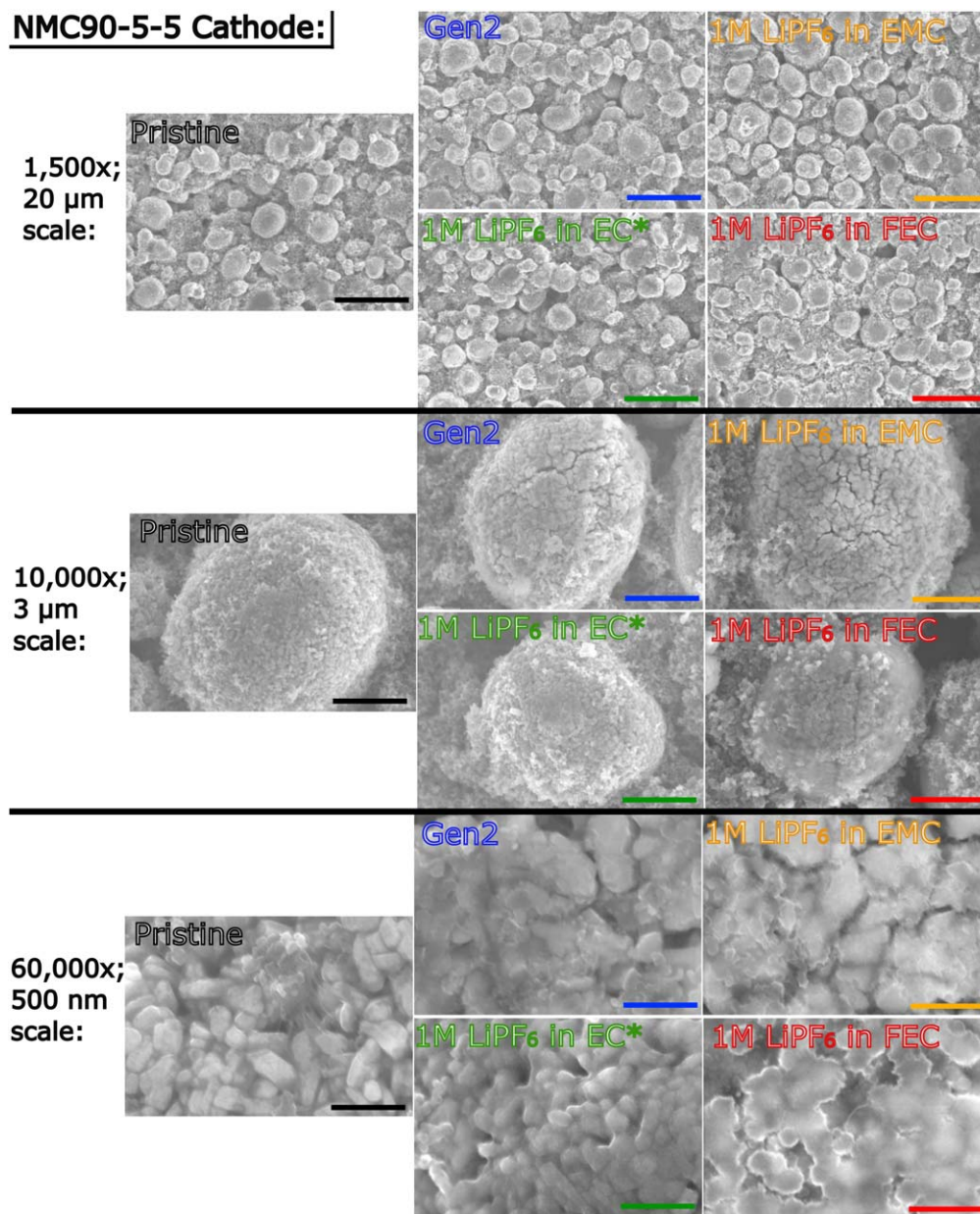


**Figure 11.** SEM images of the electrode microstructure (top), a single secondary particle (middle), and several primary particles (bottom) from the pristine NMC90-5-5 cathode and NMC90-5-5 cathodes from full cells cycled according to the BTMS cycle life protocol, terminated at 2.7V, with Gen2, 1M LiPF<sub>6</sub> in EMC, 1M LiPF<sub>6</sub> in EC, and 1M LiPF<sub>6</sub> in FEC electrolytes. \*Cells with 1M LiPF<sub>6</sub> in EC failed before reaching 400 cycles.

electrolytes (Figs. 3 and 4). ASI growth for the FEC cells shows the least impact from switching to the higher termination voltage (Figs. 5 and 6). The post-mortem half cell analysis shows minimal impact from the protocol used (Fig. 7). And the SEM of the NMC90-5-5 shows a relatively continuous, thick surface film, while the LTO film is porous and seemingly susceptible to continued surface reactions (Figs. 10 and 11). FEC's unique benefit of protecting the cathode is important as it would enable access to the higher 2.7V capacity, without a significant hit to capacity retention. However, it comes with the tradeoff of the initial loss of Li inventory and significant degradation happening at the LTO/electrolyte interphase.

*1M LiPF<sub>6</sub> in EMC.*—1M LiPF<sub>6</sub> in EMC had mixed performance in this study. In the rate test (Fig. 1), the cells with EMC-based electrolyte essentially tied for the top performance, consistent with literature that suggests EMC-based electrolytes have fast Li-ion transport.<sup>37</sup> This is also supported by the low initial ASI for the cells

with EMC-based electrolyte (Figs. 5 and 6). Under the 2.6V cycling protocol (Fig. 2), the cells with EMC-based electrolyte performed essentially the same as the cells with EC-electrolyte at 1C and a little worse at the C/10 checkup cycles. However, the similar performance was by coincidence, as their degradation mechanisms differed. EMC does not provide the benefit of passivating the LTO. This is suggested by the low-voltage peak shift in the dQ/dV profile (Fig. 3), the thin and/or porous SEI that is evident from the strong Ti 2p peak in the XPS spectra on the LTO (Fig. 8), and the SEM where the LTO cycled in EMC was the most like the pristine LTO (Fig. 10). Where EMC compensates to maintain similar degradation to the EC-based cells in the 2.6V protocol is its relatively better high-voltage stability. Again, in the 2.6V dQ/dV profile (Fig. 3), the higher voltage peaks that are associated with the cathode degradation are maintained. In the post-mortem half cell analysis of the 2.6V cells (Fig. 7), the NMC90-5-5 from EMC cells maintained a relatively higher capacity.

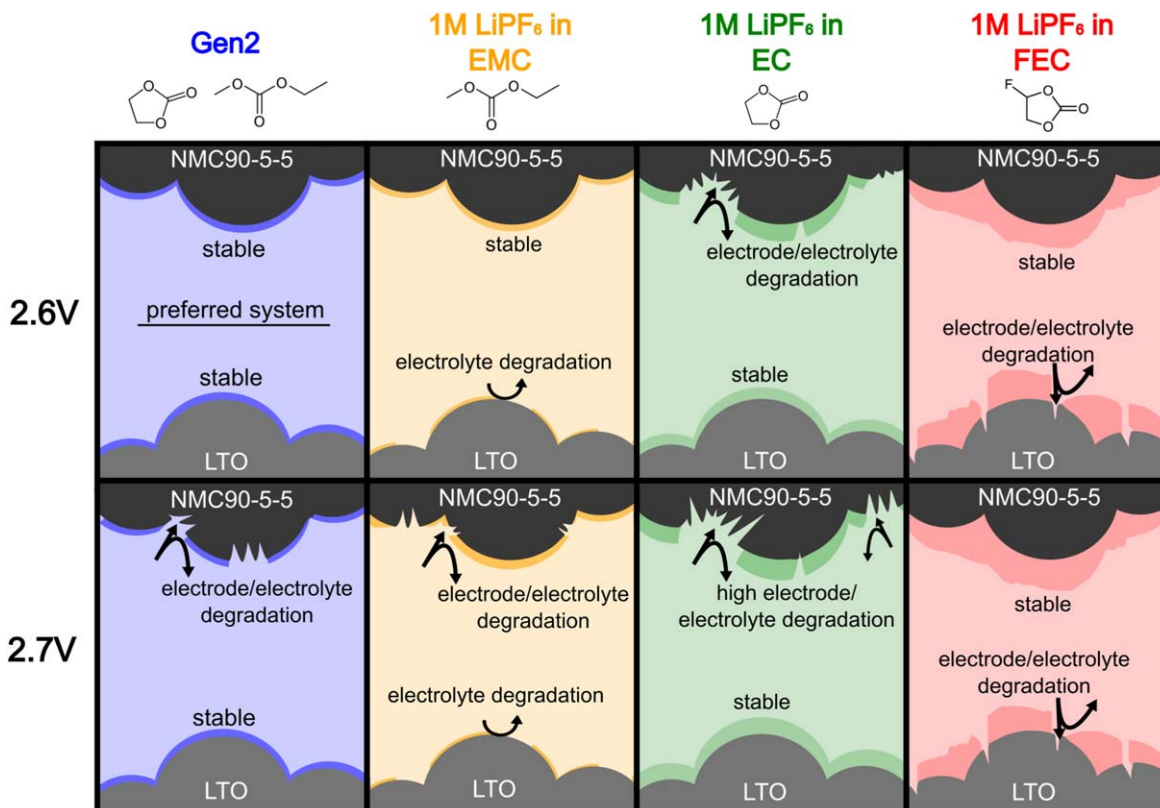


**Figure 12.** Illustration of the cycling-related performance observed in this study.

When moving to the 2.7V protocol, the EMC capacity retention suffered, but was still able to finish the protocol unlike the EC cells. Post-mortem half cell analysis (Fig. 7) shows that when moving to the 2.7V protocol, additional capacity loss happens at the cathode, as the NMC90-5-5 capacity drops significantly. From the dQ/dV plots (Figs. 3 and 4) it appears that all higher-voltage peaks will degrade in the 2.7V protocol and not just the new H2→H3 peak. It is hypothesized that the H3 phase may be more reactive with electrolyte or may mechanically degrade the NMC90-5-5/electrolyte interphase to allow fresh surface exposure and continual parasitic reactions throughout cycling. Evidence of this includes the visually-observed flaky surface film on the NMC90-5-5 in the SEM (Fig. 11) as well as the significant growth in ASI under the 2.7V protocol (Fig. 6). The lack of LTO passivation and presence of high-voltage degradation under the 2.7V protocol renders EMC alone unsuitable for BTMS applications.

**1M LiPF<sub>6</sub> in EC.**—1M LiPF<sub>6</sub> in EC was also not a top performing electrolyte in this study, but the unique benefits of EC were observed. The EC-based electrolyte displayed some Li transport limitations, evidenced by the slightly lower performance in the rate test (Fig. 1) and the difference between C/10 and 1C capacities during cycling (Fig. 2). Prior literature has indicated that the presence of EC may help with the passivation of LTO.<sup>4</sup> In the dQ/dV plots (Figs. 3 and 4) the cells with non-EC containing electrolyte show a shift of the low voltage peak associated with loss of lithium inventory via electrolyte degradation at the LTO surface. This peak is most preserved in the cells with EC-containing electrolytes. In the post-mortem half cell analysis (Fig. 7), the highest capacity LTO comes from the cell cycled with EC-based electrolyte. The mechanism of this benefit is hypothesized: the EC decomposition products help to form a stable passivation layer on the LTO, which is supported by the lack of a Ti 2p peak in the XPS analysis (Fig. 8) as well as the visual observation of a thick, continuous film on the partially cycled LTO electrode (Fig. 10).

Prior literature has also indicated that EC does not perform well at high-voltages, which is also supported by this study.<sup>35,36</sup> When moving from the 2.6V to 2.7V protocols, cells with EC-based electrolyte were the only ones to fail before reaching the end of the cycling test. It can be reasonably assumed that if the only difference was the upper termination voltage, the added degradation mechanism would be related to the high voltage cathode. Additionally, when looking at the dQ/dV plot from the 2.6V protocol (Fig. 3), a decrease of the higher-voltage signals is observed, which can be associated with degradation at the NMC90-5-5. Unfortunately, limitation in higher voltage performance would also limit accessible capacity for BTMS applications.

**Gen2 (1.2M LiPF<sub>6</sub> in 3:7 wt% EC/EMC).**—The highly-engineered Gen2 electrolyte intuitively shows performance characteristics of the previously discussed EC and EMC-based electrolytes. The cells with Gen2 electrolyte performed as well as the EMC-based cells in the rate test, if not slightly better (Fig. 1). In the cycle life test (Fig. 2), Gen2 cells performed better than all electrolytes in each metric with the exception of performing worse than the FEC-based electrolyte under the 2.7V protocol in terms of capacity retention. The dQ/dV profiles from the 2.6V protocol show that the Gen2 electrolyte doesn't seem to have significant shift or degradation of low and high voltage peaks, suggesting that Gen2 is getting the previously-mentioned benefits from both EC and EMC. However, in the 2.7V protocol (Fig. 4), similar degradation of the high-voltage peaks is seen in Gen2 cells that was seen in the EMC-based cells. Accordingly, other similarities are seen including a drop to the NMC90-5-5 half cell capacity (Fig. 7) and an increase to the ASI (Figs. 5 and 6). The low capacity retention in the 2.7V protocol renders the electrolyte unfit for that system. However, the Gen2-based cells in the 2.6V protocol showed the highest performance among all cells, exhibiting the most promising stability to perform well in BTMS applications. Using FEC as an additive for Gen2 electrolyte could be a promising approach to maintain benefits of Gen2 and preserve the cathode when cycling under the 2.7V protocol.

## Conclusions

The role of electrolyte solvent on cycle life of LTO/NMC90-5-5 batteries for BTMS applications is explored in this study. Evidence has been shown that agree with previous observations regarding the role of EC and EMC in electrolyte when paired with BTMS-relevant battery chemistries like LTO. EC exhibits an important passivating quality at the LTO/electrolyte interface, improving capacity retention, but suffers from poor stability at high voltages. EMC displays relatively better stability at high voltages, leading to less electrolyte decomposition at the NMC90-5-5/electrolyte interface. Gen2 electrolyte, containing both EC and EMC as co-solvents, seemingly benefits from both solvents' advantages and showed the highest accessible capacity throughout cycling. A significantly higher capacity can be achieved when moving from an upper termination voltage of 2.6V to 2.7V, allowing access to NMC90-5-5's H2→H3 phase change. However, this results in a significantly decreased capacity retention. From this study, to optimize cycle life for BTMS applications it is suggested that LTO/NMC90-5-5 cells should be assembled with the Gen2 electrolyte and cycled under the 2.6V protocol. Increased capacity is still desirable in terms of system-level cost and the ability to deploy BTMS in space-constrained applications; therefore, future work will include a deeper investigation of the NMC90-5-5 H2→H3 phase change.

The FEC shows high reactivity during initial formation and cycling, leading to a significant drop to accessible capacity at beginning-of-life. This causes the FEC to underperform compared to the other electrolyte solvents and not be recommended under the conditions used in this study. However, despite the poor performance, the FEC displays the unique capability to successfully passivate the NMC90-5-5/electrolyte interface when cycling to the 2.7V termination voltage and accessing the H2→H3 phase change. Therefore, studies using Ni-rich NMC may find value in incorporating FEC solvent in Gen2 electrolyte for improved capacity retention. Future research may look to avoid the high initial reactivity of FEC by building upon co-solvent design strategies<sup>23,38,39</sup> or utilizing LTO electrode surface passivation methods. On the other hand, future research may compensate for the depletion of Li-inventory by using commercially viable pre-lithiation techniques.

## Acknowledgments

This work was authored, in part, by the National Renewable Energy Laboratory (NREL), operated by Alliance for Sustainable Energy, LLC, for the U.S. Department of Energy (DOE) under Contract No. DE-AC36-08GO28308. Funding was provided by the U.S. Department of Energy's Vehicle Technologies Office under the Behind-the-Meter Storage (BTMS) Consortium directed by Fernando Salcedo and managed by Anthony Burrell. Argonne National Laboratory ("Argonne") is operated by UChicago Argonne, LLC for the U.S. DOE under Contract DE-AC02-06CH11357. The electrodes used in this paper are from Argonne's Cell Analysis, Modeling and Prototyping (CAMP) Facility, which is supported by the DOE Vehicle Technologies Office (VTO). The views expressed in the article do not necessarily represent the views of the DOE or the U.S. Government. The U.S. Government retains and the publisher, by accepting the article for publication, acknowledges that the U.S. Government retains a nonexclusive, paid-up, irrevocable, worldwide license to publish or reproduce the published form of this work, or allow others to do so, for U.S. Government purposes.

Cathode precursor synthesis reported in this paper was performed at the Materials Engineering Research Facility (MERF), Argonne National Laboratory (ANL). The MERF was supported by the DOE, Office of Energy Efficiency and Renewable Energy, and the Vehicle Technologies Office.

## ORCID

Drew J. Pereira <https://orcid.org/0000-0003-3096-2756>  
Maxwell C. Schulze <https://orcid.org/0000-0001-8368-4054>

Yeyoung Ha <https://orcid.org/0000-0003-2679-2539>  
Yicheng Zhang <https://orcid.org/0000-0002-0305-2477>  
Jihyeon Gim <https://orcid.org/0000-0002-4171-3707>  
Stephen E. Trask <https://orcid.org/0000-0002-0879-4779>  
Ozgenur Kahvecioglu <https://orcid.org/0000-0002-3988-3301>  
Glenn R. Teeter <https://orcid.org/0000-0001-8202-8477>  
Katharine L. Harrison <https://orcid.org/0000-0002-5807-6919>

## References

1. A. K. Burrell, *Behind-The-Meter Storage*, National Renewable Energy Laboratory (2021).
2. Y. Ha, S. E. Trask, Y. Zhang, A. N. Jansen, and A. K. Burrell, *J. Electrochem. Soc.*, **170**, 050520 (2023).
3. Y. Ha, A. M. Colclasure, S. E. Trask, S. Ahmed, K. L. Gering, A. N. Jansen, A. K. Burrell, and K. Park, *J. Electrochem. Soc.*, **168**, 110536 (2021).
4. Y. Ha, S. P. Harvey, G. Teeter, A. M. Colclasure, S. E. Trask, A. N. Jansen, A. K. Burrell, and K. Park, *Energy Storage Mater.*, **38**, 581 (2021).
5. H. Zhao, "Lithium Titanate-Based Anode Materials." *Rechargeable Batteries: Materials, Technologies, and New Trends* (Springer, New York) 157 (2015).
6. X. Sun, Z. Liu, F. Zhao, and H. Hao, *Environ. Sci. Technol.*, **55**, 12180 (2021).
7. B. Kumar, R. R. Srivastava, and S. P. Barik, *Miner. Eng.*, **202**, 108289 (2023).
8. C. Wu, M. Xu, C. Zhang, L. Ye, K. Zhang, H. Cong, L. Zhuang, X. Ai, H. Yang, and J. Qian, *Energy Storage Mater.*, **55**, 154 (2023).
9. A. Ghosh and F. Ghamouss, *Front. Mater.*, **7**, 186 (2020).
10. X. Feng, M. Ouyang, X. Liu, L. Lu, Y. Xia, and X. He, *Energy Storage Mater.*, **10**, 246 (2018).
11. G. Xu, P. Han, S. Dong, H. Liu, G. Cui, and L. Chen, *Coord. Chem. Rev.*, **343**, 139 (2017).
12. Z. Chen, I. Belharouak, Y. K. Sun, and K. Amine, *Adv. Funct. Mater.*, **23**, 959 (2013).
13. C. Sandhya, B. John, and C. Gouri, *Ionics*, **20**, 601 (2014).
14. O. S. Mendoza-Hernandez, H. Ishikawa, Y. Nishikawa, Y. Maruyama, and M. Umeda, *J. Power Sources*, **280**, 499 (2015).
15. D. Guittet, P. Gasper, M. Shirk, M. Mitchell, M. Gilleran, E. Bonnema, K. Smith, P. Mishra, and M. Mann, *J. Energy Storage*, **82**, 110568 (2024).
16. "Notice of the Final Determination on 2023 DOE Critical Materials List." *Federal Registration*, 516 (2023). <https://www.federalregister.gov/documents/2023/08/04/2023-16611/notice-of-final-determination-on-2023-doe-critical-materials-list>.
17. Y. Zhang, G. Teeter, Y. J. Kim, A. K. Burrell, and K. Park, *J. Energy Storage*, **64**, 107226 (2023).
18. Y. Zhang, G. Teeter, Y. J. Kim, K. Park, A. K. Burrell, and Y. Ha, *J. Electrochem. Soc.*, **170**, 090521 (2023).
19. Y. Zhang, G. Teeter, N. S. Dutta, S. Frisco, and S. D. Han, *Chem. Eng. J.*, **460**, 141239 (2023).
20. S. S. Zhang, *Energy Storage Mater.*, **24**, 247 (2020).
21. A. Manthiram, B. Song, and W. Li, *Energy Storage Mater.*, **6**, 125 (2017).
22. K. E. Kim, J. Jeong, Y. Lee, H. Lim, K. Y. Chung, H. Kim, and S. O. Kim, *J. Power Sources*, **601**, 234300 (2024).
23. B. Wang, J. Gim, S. B. Son, I. A. Shkrob, D. P. Abraham, S. E. Trask, Y. Qin, O. Kahvecioglu, A. N. Jansen, and C. Liao, *J. Electrochem. Soc.*, **170**, 020505 (2023).
24. K. Wu, L. Qian, X. Sun, X. Lei, N. Wu, H. Zhao, and Y. Zhang, *Electrochim. Acta*, **260**, 40 (2018).
25. S. J. An, J. Li, C. Daniel, D. Mohanty, S. Nagpure, and D. L. Wood III, *Carbon*, **105**, 52 (2016).
26. M. E. Spahr, H. Wilhelm, T. Palladino, N. Dupont-Pavlovsky, D. Goers, F. Joho, and P. Novak, *J. Power Sources*, **119**, 543 (2003).
27. S. Klein, S. van Wickeren, S. Roser, P. Barmann, K. Borzutzki, B. Heidrich, M. Borner, M. Winter, T. Placke, and J. Kasnatscheew, *Adv. Energy Mater.*, **11**, 2003738 (2021).
28. W. Li, A. Dolocan, J. Li, Q. Xie, and A. Manthiram, *Adv. Energy Mater.*, **9**, 1901152 (2019).
29. L. Ma, S. Glazier, R. Petibon, J. Xia, J. M. Peters, Q. Liu, J. Allen, R. Doig, and J. Dahn, *J. Electrochem. Soc.*, **164**, A5008 (2016).
30. T. Hou, G. Yang, N. N. Rajput, J. Self, S. W. Park, J. Nanda, and K. A. Persson, *Nano Energy*, **64**, 103881 (2019).
31. J. Liu, L. Zhou, W. Yu, and A. Yu, *J. Alloys Compd.*, **812**, 152064 (2020).
32. S. Aryal, J. L. Durham, A. L. Lipson, K. Z. Pupek, and O. Kahvecioglu, *Electrochim. Acta*, **391**, 138929 (2021).
33. D. J. Pereira, H. A. McRay, S. S. Bopte, and G. Jalilvand, *ACS Appl. Mater. Interfaces*, **16**, 5745 (2024).
34. K. N. Wood and G. Teeter, *ACS Appl. Energy Mater.*, **1**, 4493 (2018).
35. L. Xing, W. Li, C. Wang, F. Gu, M. Xu, and C. Yi, *J. Phys. Chem. B*, **113**, 16596 (2009).
36. M. Metzger, P. Walke, S. Solchenbach, G. Salitra, D. Aurbach, and H. A. Gasteiger, *J. Electrochem. Soc.*, **167**, 160522 (2020).
37. H. K. Bezab, S. F. Chiu, T. M. Hagos, M. C. Tsai, Y. Nikodimos, H. G. Redda, W. N. Su, and B. J. Hwang, *J. Power Sources*, **494**, 229760 (2021).
38. M. Shen, Z. Dai, L. Fan, H. Fu, Y. Geng, J. Guan, F. Sun, A. M. Rao, J. Zhou, and B. Lu, *Natl. Sci. Rev.*, **11**, nwa359 (2024).
39. D. Liu, L. Yuan, X. Li, J. Chen, R. Xiong, J. Meng, S. Zhu, and Y. Huang, *ACS Appl. Mater. Interfaces*, **14**, 17585 (2022).